Mémoire

Auteur : Dekoster, Lise
Promoteur(s) : 24259; Beckers, Jean-Marie
Faculté : Faculté des Sciences
Diplôme : Master en océanographie, à finalité approfondie
Année académique : 2023-2024
URI/URL : http://hdl.handle.net/2268.2/21041

The Influence of Freshwater Runoff around the Antarctic Continent on the Meridional Overturning Circulation

Lise Dekoster

Promotor: Professor Petteri Uotila[1]

Co-promotor: Professor Jean-Marie Beckers[2]

A thesis presented for the degree of

Master in Oceanography

University of Liège (Belgium)

Academic year 2023-2024

[1]Institute for Atmospheric and Earth System Research (INAR), University of Helsinki.
[2]GeoHydrodynamics and Environment Research (GHER), University of Liège.

Jury members

Petteri Uotila (Promotor)

Jean-Marie Beckers (Co-promotor)

Alexander Barth

Alberto Borges

Loïc Michel

According to the rules imposed by the jury of the Master in Oceanography, this document must not exceed 50 pages in Times 12 or an equivalent font.

Acknowledgements

Firstly, I would like to express my gratitude towards professor Beckers and professor Uotila for accepting my request to be my promotors. In particular, I am very grateful to professor Uotila for making my stay at the University of Helsinki possible. During these four months, his kindness, scientific insights, patience, daily supervision and endless support, were really indispensable for making this thesis.

I also would like to thank everyone at the Institute of Atmospheric and Earth System Research for welcoming me so dearly. I really felt their warmth and inclusiveness, which created a little family far from home.

I also wish to thank Andreas, for his support, help and love during these four months, but also during my whole education. To Cèlia who always cheered me up and believed in me. I also would like to express my thanks to my sister for pointing out problems in my thesis.

Ook zou ik mijn ouders willen bedanken om mij al deze jaren te steunen. Zonder hen zou ik niet staan waar ik nu stond. Ik zou ook graag meme bedanken om mij de waarde van onderwijs bij te brengen en mij onvoorwaardelijk te steunen en te helpen doorheen mijn leven.

I also would like to thank my readers, professor Barth, professor Borges and professor Michel, for taking the time to read my thesis.

Lastly, I would like to express my gratitude towards all the professors in the Master's program in Oceanography. They taught me how complex, magnificent and crucial the oceans are. I will cherish this for my entire life.

Abstract

The Global Meridional Overturning Circulation (GMOC) is a global ocean circulation that redistributes heat, freshwater and nutrients around the globe. It plays an important role in climate, biogeochemical cycling and marine ecosystems. This thesis investigates the effect of Antarctic meltwater runoff in the Southern Ocean on the Meridional Overturning Circulation in the Atlantic basin with a global ocean model, the Nucleus for European Modelling of the Ocean (NEMO). We find a *weakening* of the Antarctic Bottom Water (AABW) circulation and an *increase* in the North Atlantic Deep water circulation. Moreover, we find that the abyssal ocean is warming. Lastly, we find important sea surface temperature and sea surface salinity signals in the North Atlantic, North Pacific and the El Niño region.

Résumé

La circulation méridienne globale de retournement est une circulation océanique globale qui redistribue la chaleur, l'eau douce et les nutriments autour du globe. Elle joue un rôle important dans le climat, les cycles biogéochimiques et les écosystèmes marins. Ce mémoire étudie l'effet du ruissellement des eaux de fonte de l'Antarctique dans l'océan Austral sur la circulation méridienne de retournement dans le bassin de l'Atlantique à l'aide d'un modèle océanique global, le Nucleus for European Modelling of the Ocean (NEMO). Nous constatons un *affaiblissement* de la circulation des eaux de fond de l'Antarctique (AABW) et un *augmentation* de la circulation des eaux profondes de l'Atlantique Nord. En outre, nous constatons un réchauffement de l'océan abyssal. Enfin, nous trouvons d'importants signaux de température et de salinité de surface de la mer dans l'Atlantique Nord, le Pacifique Nord et la région El Niño.

List of Abbreviations

AABW	Antarctic Bottom Water
AAIW	Antarctic Intermediate Water
ACC	Antarctic Circumpolar Current
AMOC	Atlantic Meridional Overturning Circulation
CDW	Circumpolar Deep Water
ENSO	El Niño–Southern Oscillation
IDW	Indian Deep Water
IPCC	Intergovernmental Panel on Climate Change
LCDW	Lower Circumpolar Deep Water
MOC	Meridional Overturning Circulation
NADW	North Atlantic Deep Water
NEMO	Nucleus for European Modelling of the Ocean
PDW	Pacific Deep Water
RCP	Representative Concentration Pathways
SAMW	Subantarctic Mode Water
SMOC	Southern Ocean Meridional Overturning Circulation
SO	Southern Ocean
SSS	Sea Surface Salinity
SST	Sea Surface Temperature
Sv	Sverdrup
UCDW	Upper Circumpolar Deep Water

Contents

1 Introduction **1**

2 Background **4**

2.1 The Global Meridional Overturning Circulation 4

2.2 Drivers of Meridional Ocean Circulation 6

2.2.1 Thermohaline dynamics 6

2.2.2 Wind-driven dynamics 7

2.3 The Meridional Overturning Circulation in the Atlantic Basin 8

2.3.1 Schematic representation 8

2.4 The Southern Ocean 10

2.4.1 Description 10

2.4.2 Antarctic Bottom Water 12

2.4.3 Importance 13

2.4.4 Climate Change and the Antarctic Ice Sheet 14

2.4.5 Challenges 15

3 Material and methods **16**

3.1 Model description 16

3.2 Model initialization 17

3.3 Mathematical formulation 18

3.3.1 Ocean circulation 18

3.3.2 The meridional overturning streamfunction 20

3.4 Methodology 21

4 Results **24**

4.1 The Meridional Overturning Circulation in the Atlantic Basin 24

4.1.1 Yearly average transport 24

4.2 Time evolution of the Meridional Overturning Circulation in the Atlantic Basin 26

4.3 Impact on Southern Ocean 28

4.3.1 Yearly average of SST and SSS 28

4.3.2 Surface downward heat flux . . . 29
4.3.3 Sea ice concentration in February and September . . . 30
4.3.4 Yearly average sea bottom temperature . . . 32
4.4 Impact on global ocean . . . 33
4.4.1 Yearly average of SST and SSS . . . 33
4.4.2 Yearly averaged surface downward heat flux . . . 35
4.4.3 Decadal average sea surface temperature . . . 37
4.4.4 Yearly average sea bottom temperature . . . 37

5 Discussion **39**

5.1 Comparison between the model output of the Meridional Overturning Circulation in the Atlantic Basin and observations . . . 39
5.2 Influence of freshwater on the Meridional Overturning Circulation in the Atlantic Basin . . . 40
5.2.1 Time evolution . . . 40
5.2.2 Comparison with literature . . . 40
5.3 Abyssal warming . . . 41
5.4 Yearly vs decadal SST and SSS . . . 42
5.5 Sea ice concentration and ecosystems . . . 42
5.6 Anomalies in the equatorial Pacific and the north Pacific . . . 43
5.6.1 Warm Blob? . . . 43
5.6.2 The equatorial Pacific . . . 44
5.6.3 North Pacific . . . 46

6 Conclusion and future work **47**

1 Introduction

Ocean currents play a critical role in the Earth's climate. However, as a result of anthropogenic forcing, the ocean currents are altered, which exerts further pressure on the global climate. These currents are intrinsic to a fluid on a rotating, spherical body, such as the Earth. As a result of the spherical shape of the Earth, there is differential heating of the Earth's surface by the sun, with the equator receiving more heat compared to the poles. This uneven heating drives the meridional (north-south) heat transport in the ocean through global ocean circulation, known as the Global Meridional Overturning Circulation (GMOC). This is a *large-scale* circulation, which transports the excess heat together with carbon, freshwater and nutrients around the globe, affecting the climate (Lynch-Stieglitz, 2017; Rahmstorf, 2023; Svendsen et al., 2014) and marine ecosystems (Sarmiento et al., 2004).

Furthermore, the Earth's rotation generates a Coriolis force that deflects currents westward (Reid, 1994; Stommel, 1958). Lastly, the gravitational field of the Earth induces stratification within the ocean, i.e. a vertical layering of the ocean, where lighter water masses float on top of heavier water masses. The transition of temperatures between these warm surface waters and cold deep water is called the thermocline, which is a permanent feature of the ocean. At the equator, where solar radiation is most intense, the thermocline is more pronounced compared to polar regions.

In more detail, the drivers of the GMOC are the *thermohaline differences* and *wind-stress curl*, specifically in the Southern Ocean (SO) (Section 2.2). Thermohaline differences refer to the variations in temperature and salinity, which influence the density of water. This density difference controls the rising and sinking of water, which plays a key role in the overturning circulation. The poles play a crucial part in generating these thermohaline differences. In the North Atlantic Ocean, cold air temperatures generate cooling of the sea surface. As a result of an increase in density, the surface water sinks into the ocean's interior, a process known as *deep water formation*. Unlike in the northern Atlantic Ocean, deep water formation does not occur in the North Pacific (Warren, 1983). This is due to the lower salinity surface water, which leads to strong stratification which prohibits sinking to depth. The deep water formation in the

North Atlantic and the Southern Ocean results in deep currents, which together with the surface currents close the GMOC (see Section 2.3).

The GMOC can be divided per ocean basin, where the most frequently studied one is the MOC in the Atlantic basin, commonly known as AMOC (Ditlevsen and Ditlevsen, 2023; Kim et al., 2022; Sinet et al., 2023; van Westen et al., 2024). The AMOC is identified as a tipping point in Earth's climate (Lenton et al., 2008), which means that under slow forcing it can undergo a relatively rapid substantial change. For the AMOC, this forcing results from the surface warming and freshening of the Labrador, Irminger, and Greenland-Iceland-Norwegian Seas (Cheng et al., 2013; Weaver et al., 2012; Weijer et al., 2020). However, the influence of the Southern part of the GMOC does not receive the same attention. Nonetheless, under global warming the surface waters of the SO are also freshening (Bintanja et al., 2013; Swart et al., 2018; The IMBIE team, 2018), due to an increase in meltwater from runoff, ice melt, glacial melt and precipitation. This could have profound effects on the GMOC. We will therefore study the influence of the addition of freshwater in the Southern Ocean on Meridional overturning circulation in the full Atlantic Basin (Atlantic and Southern Ocean). We can define the objectives of the thesis as follows:

- The first objective is to determine if the Meridional Overturning Circulation in the Atlantic Basin is influenced by the freshening of surface water due to increased meltwater around Antarctica.
- The second objective is to assess whether the sea surface temperature (SST), sea surface salinity (SSS), sea bottom temperature, and downward heat flux are altered by increased meltwater around the Antarctic continent. This analysis will be conducted for both the Southern Ocean and the Global Ocean.
- The third objective is to examine the influence of freshwater on the sea ice formation in the Southern Ocean.

In order to address these questions, we will solely rely on a configuration of the model framework, Nucleus for European Modelling of the Ocean (NEMO). We will have a control configuration and a configuration where we add freshwater (see Figure 2).

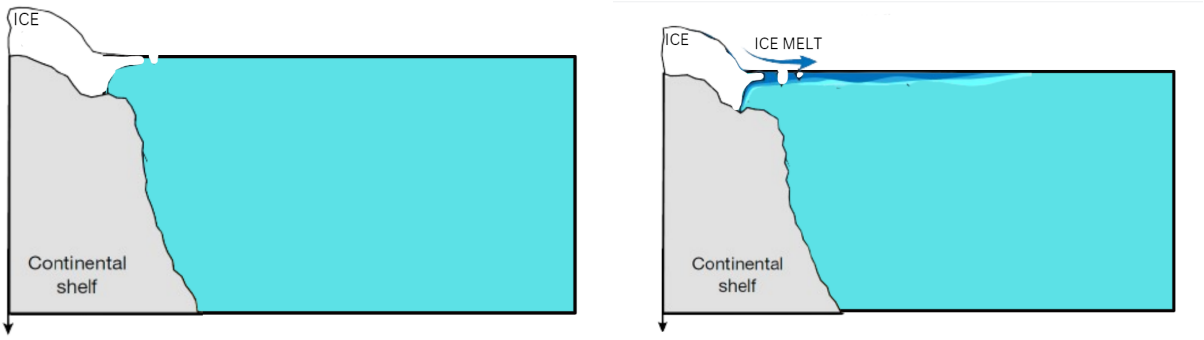

(a) Control configuration.

(a) Additional freshwater input.

Figure 2: (a) shows the control configuration. (b) shows the configuration with an increase in freshwater run-off compared to the control configuration. Figure adapted from Bronselaer et al., 2018.

The thesis is structured as follows: the first chapter is dedicated to the necessary background, including an in-depth explanation of the Meridional Overturning Circulation (see Section 2.1) and its drivers (see Section 2.2). Following this, we will introduce the Meridional Overturning Circulation, specifically in the Atlantic Basin (see Section 2.3). Next, we focus on the Meridional Overturning Circulation in the Southern Ocean. This chapter concludes with a section about the Southern Ocean, where we explain the importance of the Southern Ocean for the global ocean in terms of marine ecosystems, biogeochemistry and climate (Section 2.4.3). We introduce the effects of climate change (Section 2.4.4) and the challenges concerning observations in the Southern Ocean (Section 2.4.5).

In order to determine the effect of freshwater around the Antarctic continent on the meridional ocean circulation in the Atlantic basin, we use the global circulation model Nucleus for European Modelling of the Ocean (NEMO), which is explained in Section 3.1. We will explain some details regarding the mathematical formulation (Section 3.3) of the model and the meridional overturning streamfunction. We made two different simulations, one control configuration and one with additional freshwater input. This will be explained in the Methodology (Section 3.4). The following chapters consist of the results of the model (Section 4), the discussion (Section 5) and the conclusion (Section 6).

2 Background

2.1 The Global Meridional Overturning Circulation

The Global Meridional Overturning Circulation is a global ocean circulation that redistributes heat, salt, nutrients, O_2 and CO_2 around the globe (Atamanchu, 2021). In the North Atlantic it is responsible for heat transfer at the rate of one petawatt, which is 50 times the energy use of humankind (Rahmstorf, 2023; Trenberth et al., 2019). It influences climate globally, such as for example temperature and precipitation in Europe (Sutton and Hodson, 2005). It can also control Sahel rainfall (Martin et al., 2014) and affects the mean position of the intertropical convergence zone (Marshall et al., 2014; Orihuela-Pinto et al., 2022). Moreover, it impacts climate on interannual and decadal timescales (Orihuela-Pinto et al., 2022) and has caused abrupt climate change in the past (Rahmstorf, 2002). In addition, it could be linked with El Niño–Southern Oscillation (Orihuela-Pinto et al., 2022)

Schematically, the GMOC consists out of 4 layers: the upper ocean/thermocline layer, an intermediate layer, a deep layer and a bottom layer (Talley, 2013). The schematics of this circulation are shown in Figure 3. The ocean in the Atlantic basin is characterized by two overturning cells: the North Atlantic Deep Water cell and the Antarctic Bottom Water cell, which are connected by the Southern Ocean. In the North Pacific, there is a weak overturning cell, which is only weakly connected to the overturning cells found in the Atlantic. Next to the NADW and AABW, the other deep water masses are Pacific Deep Water and Indian Deep Water. These water masses are formed from AABW and NADW, due to the fact that they are not connected by surface waters, they have a low oxygen and high nutrient content (Talley, 2013). In the Southern Ocean, there is another deep water mass, Circumpolar Deep Water. This circumpolar deep water (CDW) forms from NADW, IDW and PDW (Talley, 2013). CDW consists of lower circumpolar deep water (LCDW) and upper circumpolar deep water (UCDW).

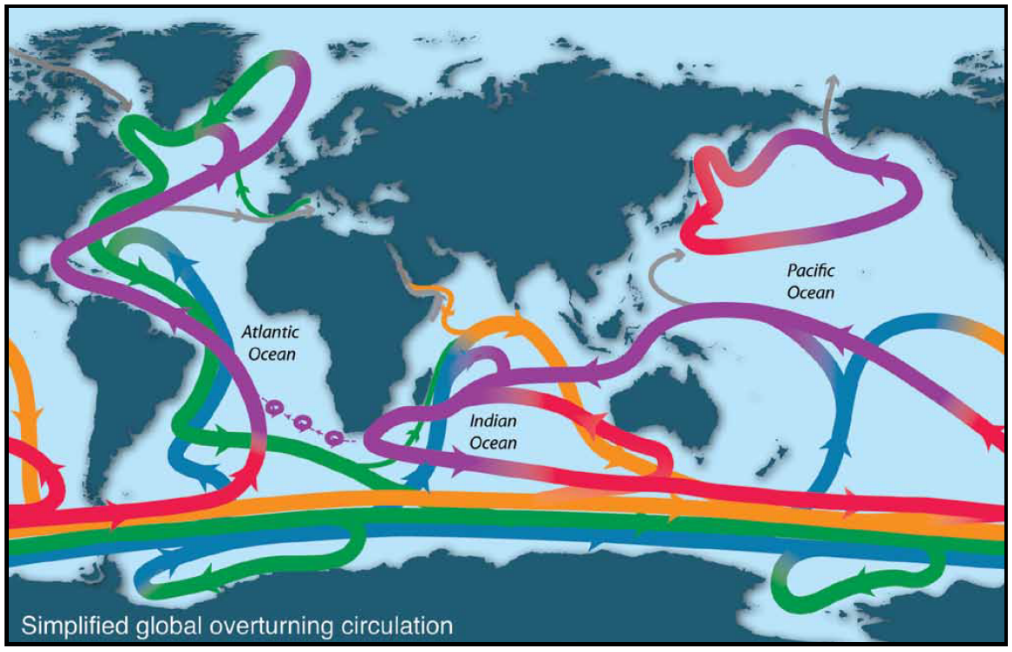

Figure 3: Global overturning circulation. Purple indicates the upper ocean and thermocline. The red colours show the denser thermocline and intermediate water. Orange is the Indian Deep Water IDW) and Pacific Deep Water (PDW). Green displays the North Atlantic Deep Water (NADW). Blue shows the Antarctic Bottom Water (AABW). Gray is the Bering Strait components and Mediterranean and Red Sea inflows. Figure taken from Talley, 2013.

2.2 Drivers of Meridional Ocean Circulation

The large-scale ocean circulation is driven by thermohaline and wind-driven dynamics. These are not isolated processes, but they work simultaneously to drive the ocean circulation.

2.2.1 Thermohaline dynamics

2.2.1.1 Deep water formation at high latitudes

At high northern latitudes, deep water is formed in the Labrador, Irminger, Greenland and Iceland seas (Killworth, 1983; Petit et al., 2020), which results in ventilation of the ocean. This means that there is contact with the atmosphere. Around the Antarctic continent, deep water is formed in the Weddell Sea (Foster and Carmack, 1976), Ross Sea (Jacobs et al., 1970), off the Adélie Coast (Williams et al., 2008) and in the Cape Darnley (Ohshima et al., 2013).

Deep water formation occurs in two main forms: continental shelf slope convection and open ocean convection (Killworth, 1979; Rudels and Quadfasel, 1991). This process leads to buoyancy loss, resulting in diapycnal downwelling. During diapycnal downwelling, water sinks vertically, crossing different isopycnals. Continental shelf slope convection is typical for deep water formation around the Antarctic continent. Here, dense water is formed on the continental shelves due to brine rejection of the ice formation in polynyas and cooling by strong cold katabatic winds. This induces a vertical movement with accompanying entrainment of the surrounding water. Once a critical density is reached, the water cascades into the abyssal ocean.

Open ocean convection occurs mainly in the Labrador and Greenland seas, and was once observed in the irregular Weddell Polynya (Gordon, 1982). During winter, strong surface cooling causes an increase in density, which causes unstable stratification. If the density of the surface water exceeds the density of the underlying water layer, a downward flow is established, which forms a chimney (Killworth, 1979; Wadhams et al., 2002).

2.2.1.2 Diapycnal upwelling at low latitudes

At low latitudes, water rises due to turbulence caused by increased temperatures, resulting in diapycnal upwelling. Diapycnal upwelling occurs when water is drawn up vertically, crossing

isopycnals by mixing. This process happens as the ocean's interior slowly warms from the heat received at the sea surface, which then diffuses to warm the ocean's interior. The diapycnal upwelling at low latitudes in the Pacific and Indian Ocean plays an important role in the Meridional Overturning Circulation in the Atlantic basin (see 2.3) (Talley, 2013).

The diapycnal upwelling depends on the eddy diffusivity (κ) (Robinson and Stommel, 1959) which is maintained by small-scale turbulence. The value is 10^{-4} ms^2 (Munk, 1966).

2.2.2 Wind-driven dynamics

The Deacon cell (Speer et al., 2000), which is the wind-driven circulation, is caused by the wind stress curl of the strong eastward flowing winds in the Southern Ocean. This generates adiabatic upwelling of Lower Circumpolar Deep Water (LCDW), which is North Atlantic Deep Water (NADW) that has been modified as a result of mixing with other locally deep water masses (Talley, 2013). The upwelling results in sloping isopycnals, which are unstable. This baroclinic instability tends to flatten out the isopycnals, which release the available potential energy (Gill et al., 1974; Vallis, 2019). This results in highly energetic eddying motions, which transport water masses towards Antarctica (Marshall and Speer, 2012). As a result of the Deacon cell, the temperature and salinity profiles are sloping towards Antarctic, as can be seen in Figure 5.

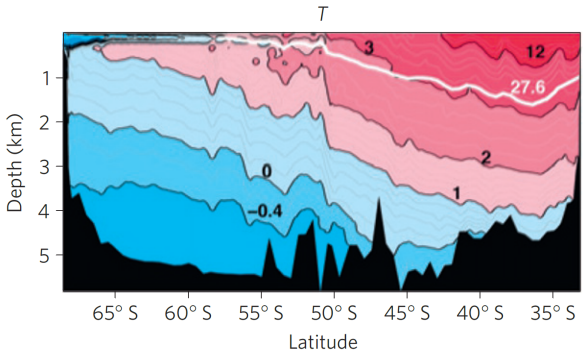

(a) Temperature profile in the Southern Ocean.

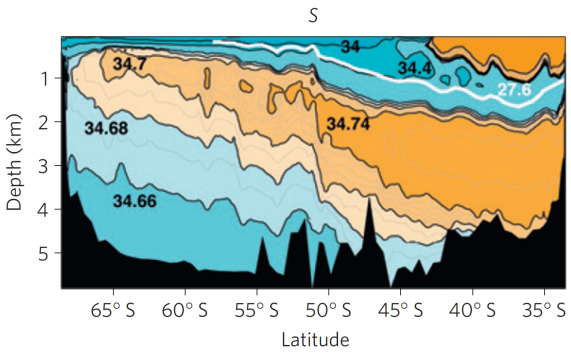

(a) Salinity profile in the Southern Ocean.

Figure 5: Temperature and salinity sections. Figure taken from Marshall and Speer, 2012

2.3 The Meridional Overturning Circulation in the Atlantic Basin

2.3.1 Schematic representation

The Meridional Overturning Circulation (MOC) in the Atlantic basin is an interhemispheric ocean circulation in the meridional vertical plane situated in the Atlantic Basin. The Atlantic Meridional Overturning Circulation (AMOC) is located in the Atlantic Ocean, the Southern Ocean Meridional Overturning Circulation (SMOC) is located in the Southern Ocean. This circulation transports heat and salt around the globe in deep and surface currents, which affects the climate globally (Talley, 2013).

This circulation consists of two meridional cells (see Fig. 6 for a simplified view). The upper cell is driven by dense water formation, in open ocean and on the shelves, caused by buoyancy loss at high northern latitudes. This North Atlantic Deep Water (NADW) is transported southward at mid-depth towards the Southern Ocean. At the Antarctic convergence, NADW resurfaces as CDW by upwelling induced by the ACC. Due to Ekman transport, the AAIW, formed through CDW, is advected toward the equator, which closes the upper cell. The lower cell consists of Antarctic Bottom Water (AABW) formed by deep water formation, mainly on the shelves. AABW sinks to the abyss of the ocean, where it flows towards the equator. Due to warming at low latitudes, it rises and mixes with the southward-flowing water. As a result of upwelling in the ACC, the water resurfaces and flows to the south due to baroclinic eddies.

In reality, the circulation is more complex, since the circulation in the Atlantic basin is in contact with the Indian and Pacific basins connected by the ACC. One part of the NADW enter the Indian Ocean, while another part forms AABW. As a result of diapycnal diffusion the AABW, which enters the Indian and Pacific Ocean, forms Pacific Deep Water (PDW) and Indian Deep Water (IDW) (Gordon, 1986). This can only happen in the Indian and Pacific Ocean since enough heat enters the deep ocean. The ACC then draws up the PWD and IDW to the surface, which flows northward due to Ekman transport (Speer et al., 2000). In the ACC there is also diapycnal mixing, but this is lower than isopycnal mixing (Garabato et al., 2016).

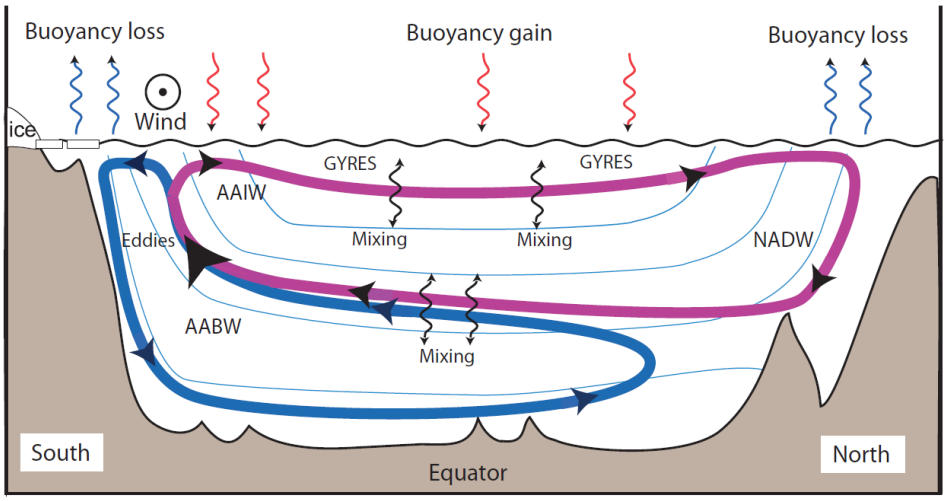

Figure 6: The meridional overturning cells. The upper cell (in purple) is rotating in a clockwise direction: the surface current is transporting heat and salt northwards, while the deep currents transport cold, dense water (NADW) toward the south. The lower cell, or the Deacon cell, (in blue) in rotating anticlockwise, transporting AABW toward the north. Figure taken from Vallis, 2019.

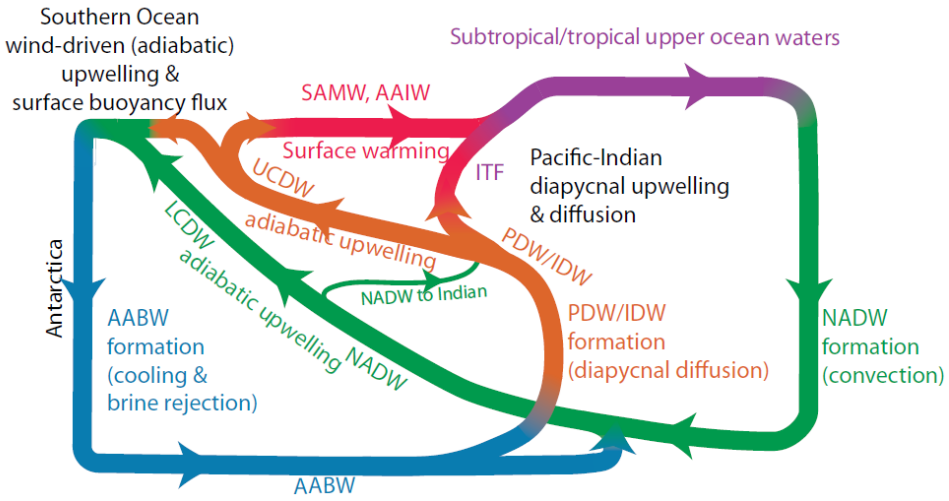

Figure 7: General view of the Meridional Overturning Circulation, including the thermohaline and wind-driven drivers. This includes the role of the diapycnal diffusion in the Indian and Pacific Ocean, which plays an important role in closing the overturning circulation in the Atlantic basin. Figure taken from Talley, 2013.

2.4 The Southern Ocean

2.4.1 Description

The area south of 35°S is defined as the Southern Ocean (Chapman et al., 2020) and encompasses the Antarctic continent. It includes the Weddell and the Ross sea, two big incisions in the Antarctic continent (see Fig. 8). The Southern Ocean is not enclosed by any continent, which results in the exchange of water masses between the Atlantic, Pacific and the Indian Ocean through the ACC. The narrowest point of the Southern Ocean is the Drake Passage, which measures 1000 km between Cape Horn and the Antarctic peninsula. The Antarctic continental shelf has a mean depth of 500 m with a variable distance from coastline to shelf break, ranging from 10 km to 100 km in the Weddell and Ross Sea. Outside the continental shelf, the depth increases to 4 km. The Southern Ocean is characterized by various abyssal plains, ridges and fracture zones (Dorschel et al., 2022), such as the Kerguelen Plateau, Campbell Plateau and the East Pacific Rise.

Between 30°S and 60°S the Southern Ocean is characterized by strong eastward flowing winds, which induce the Antarctic Circumpolar Current (ACC). Due to the absence of continents, this eastward wind-driven current forms the largest current on Earth. The ice sheets covering the Antarctic continent cause cooling of air, which results in high pressure. However, the coastal areas are characterized by low pressure. This induces strong winds, which follow the topography over the continent toward the ocean. These winds are deflected by the Coriolis force, which results in a westward flowing wind around the Antarctic continent (Parish and Bromwich, 1997), which induces a coastal current, east wind drift, in the same direction (see Fig. 8).

The Southern Ocean is characterized by extensive sea ice, which reaches a peak during the end of the austral winter, in September. The expansion is limited by the ACC. The sea ice, which is mostly first year sea ice, can freely expand due to the absence of continental borders. The sea ice cover can be interrupted by polynyas, large open areas which acts as sea ice factories, caused by strong katabatic winds which pushes sea ice away from the continent.

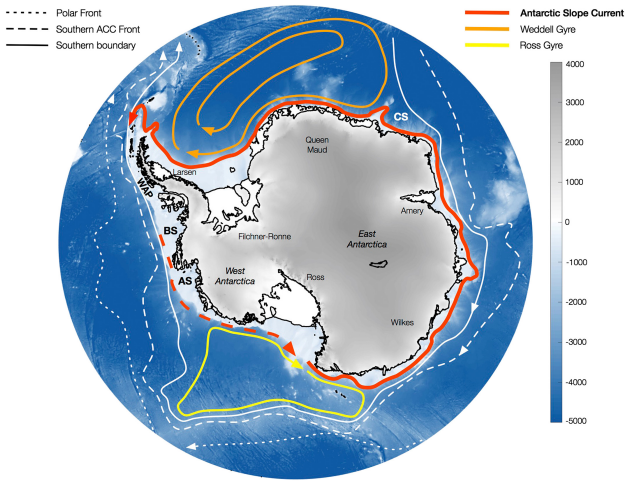

Figure 8: The Antarctic Circumpolar Current (ACC) and the westward flowing wind around the Antarctic continent. Figure taken from Thompson et al., 2018.

The water masses of the Atlantic, Pacific and Indian Ocean outflow in the Southern Ocean. Under the influence of the ACC this results in different fronts i.e. boundaries of water masses with different properties (see Figure 9). Important dynamical fronts related to the ACC are the Subantarctic Front (SF), Polar Front (PF), Southern ACC Front (SACCF) and the Antarctic Slope Front (ASF).

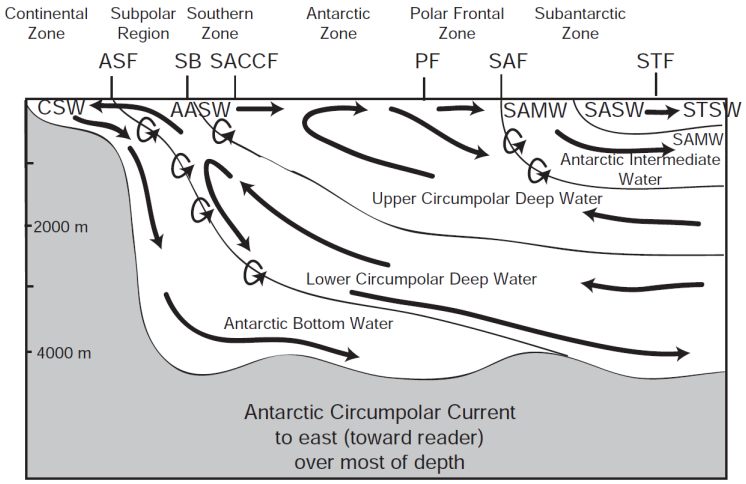

Figure 9: Transect of the Southern Ocean with the different water masses: Antarctic Bottom Water (AABW), Lower Circumpolar Deep Water (LCDW), Upper Circumpolar Deep, Continental Shelf Water (CSW), Antarctic Surface Waters (AASW), Antarctic Intermediate Water (AAIW), Subantarctic Mode Water (SAMW), Subantarctic Surface Water (SASW), Subtropical Surface Water (STSW) and the different fronts: Antarctic Slope Front (ASF), Southern Boundary (SB), Southern ACC Front (SACCF), Polar Front (PF), Subantarctic Front (SAF), Subtropical Front (STF). Figure taken from Talley, 2011.

2.4.2 Antarctic Bottom Water

Antarctic Bottom Water (AABW) plays a crucial role in the climate system, since it influences the atmospheric carbon dioxide over periods of centuries and millennia (Marzocchi and Jansen, 2019; Sigman and Boyle, 2000). The reason for this is the sinking of extremely cold and salty waters after contact with the atmosphere. As a result, it allows the ventilation of the abyssal ocean (Johnson, 2008), supplies oxygen (Gordon, 2009), and can hold heat and carbon (de Lavergne et al., 2017) at depth for centuries. Additionally, it plays an important role in the global primary production, since nutrients that are not used by marine organisms, due to iron or light limitations, are sinking to depth. This then affects the biological carbon pump (Marinov et al., 2006).

A diagram of the formation of AABW is displayed in Figure 10. An important role in the formation of AABW is played by the ice formation in polynyas. Due to the brine rejection and heat loss, the water becomes extremely cold and salty, known as high-salinity shelf water. Next, this water is further cooled, resulting in supercooled water, which is colder than the freezing point of the water at the surface ($< -2°C$), known as Ice Shelf Water. These dense shelf waters then cascade into the abbysal ocean, where it mixes with other water masses such as circumpolar deep water, forming Antarctic Bottom Water.

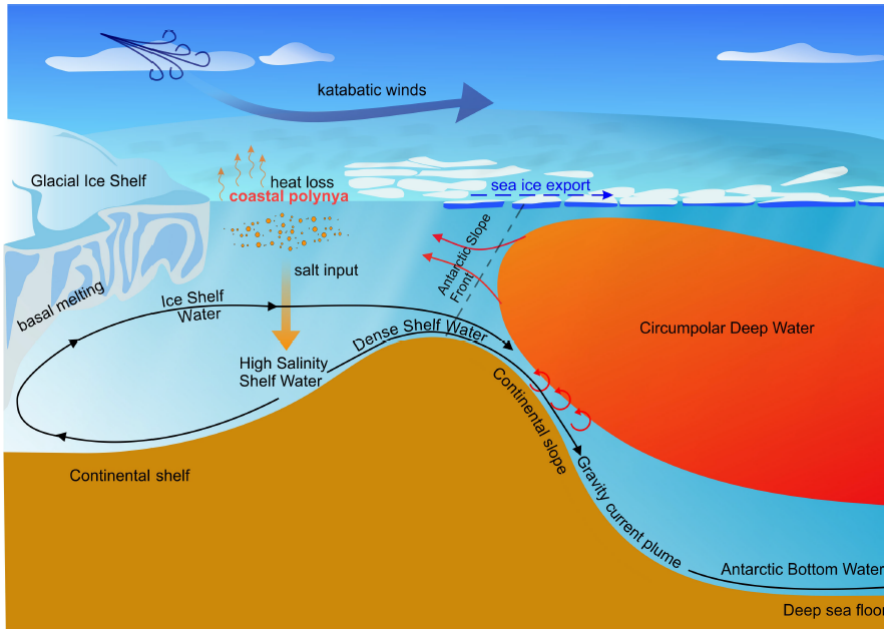

Figure 10: Schematic overview of the formation of Antarctic Bottom Water. Figure taken from Silvano et al., 2023

2.4.3 Importance

The Southern Ocean plays an important role in reducing global warming. This is due to the strong upwelling zones; the upwelled water from the deep ocean is very cold and low in CO_2. Due to contact with the atmosphere, it takes up large amounts of heat and CO_2 (Khatiwala et al., 2009; Manabe et al., 1991; Mikaloff-Fletcher et al., 2006), which end up in the ocean's interior. Thus, it acts as a sink for anthropogenic CO_2 and heat. From 1861 to 2005, the Southern Ocean below 30° S accounted for 43 % of anthropogenic CO_2 uptake and 75 % of heat uptake (Frölicher et al., 2015) of the excess heat and CO_2 which the ocean absorbs.

The Southern Ocean also plays an important role in the biological productivity at low latitudes. This is because Subantarctic Mode Water (SAMW), rich in nitrate formed in the Southern Ocean, spreads throughout the Southern Hemisphere and the North Atlantic Ocean providing nutrients for the thermocline in the entire Southern Hemisphere and the North Atlantic Ocean (Sarmiento et al., 2004). Moreover, it takes up carbon, as it brings carbon from the surface ocean to the abyssal ocean. It also plays a role in the biogeochemical cycling of nitrate and phosphate. From a biological perspective, the Southern Ocean is rich in various ecosystems

due to the many fronts (Chapman et al., 2020). Figure 11 gives an overview of the interaction between the physical, chemical and biological processes which occur in the SO.

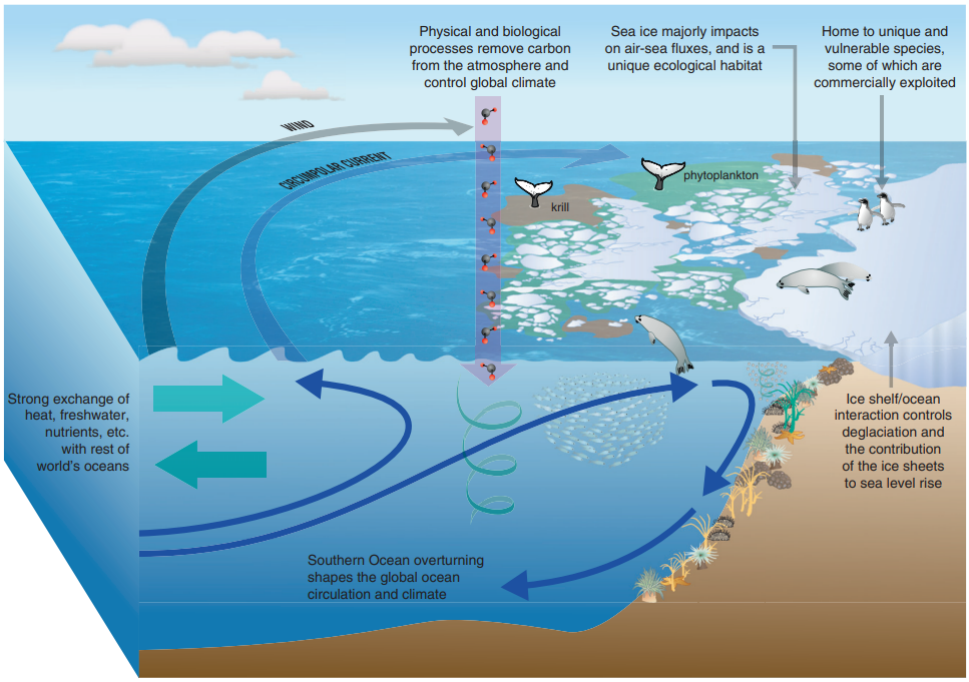

Figure 11: Overview of the interactions between physical and biological processes. Figure taken from Meredith et al., 2013.

2.4.4 Climate Change and the Antarctic Ice Sheet

Global warming accelerates the mass loss of the Antarctic Ice sheet (Konrad et al., 2018; Paolo et al., 2015; Wouters et al., 2015). This mass loss is driven by melting of ice shelves due to warmer ocean waters (Pritchard et al., 2012), as a result the Southern Ocean is freshening, as shown by observations (de Lavergne et al., 2014; Durack and Wijffels, 2010; Durack et al., 2012; Skliris et al., 2014). The meltwater induces subsurface warming, which leads to further ice-sheet and ice-shelf melt (Bronselaer et al., 2018). The increase of meltwater increases sea ice (Bintanja et al., 2013). The freshening of surface water increases the stratification and thus decreases the mixed layer.

2.4.5 Challenges

The observations in the Southern Ocean are sparse due to its remoteness and harsh conditions, particularly in winter. This leads to extremely sparse surface observations of Antarctic sea ice thickness (Worby et al., 2008), snow thickness on sea ice, ocean temperature and salinity. Moreover, observations of currents, especially under the sea ice and in ice shelf cavities, are also sparse.

Due to the important role of the Southern Ocean on the Meridional Overturning Circulation, the Earth's heat and freshwater balances, and the stability of the Antarctic ice sheet, efforts are made to increase the measurements in the Southern Ocean. An example of such an initiative is the Southern Ocean Observing System (Meredith et al., 2013). In addition to this, autonomous instruments such as Argo buoys (Dong et al., 2008) and elephant seals (*Mirounga leonina*) (Charrassin et al., 2008) are used to increase the in-situ observations.

3 Material and methods

3.1 Model description

In order to assess the influence of freshwater around the Antarctic continent on the meridional overturning circulation in the Atlantic basin, SST, SSS and sea ice formation, we have chosen to use the Nucleus for European Modelling of the Ocean (NEMO). This is a state-of-the-art modelling framework in which one can model the ocean dynamics, the sea ice and the biogeochemistry and their interaction. This framework is written in FORTRAN and has three major components:NEMO-OPA (ORCA) (Madec et al., 2023), NEMO-SI³ (Vancoppenolle et al., 2023) (ICE), NEMO-TOP (Tracer in the Ocean Paradigm)(Group, 2018) (PISCES). NEMO-OCE is the physical ocean component of the model, which models the ocean dynamics and thermodynamics. NEMO-SI³ models the sea-ice dynamics and thermodynamics. NEMO-TOP models the biogeochemistry.

We used ORCA2-ICE-PISCES, a *global* ocean configuration which is run together with the SI3 model and the PISCES biogeochemical model. The ORCA2 grid is a tripolar, which allows the construction of a global orthogonal curvilinear ocean mesh (see Figure 12) with no singular points (Madec et al., 2023).

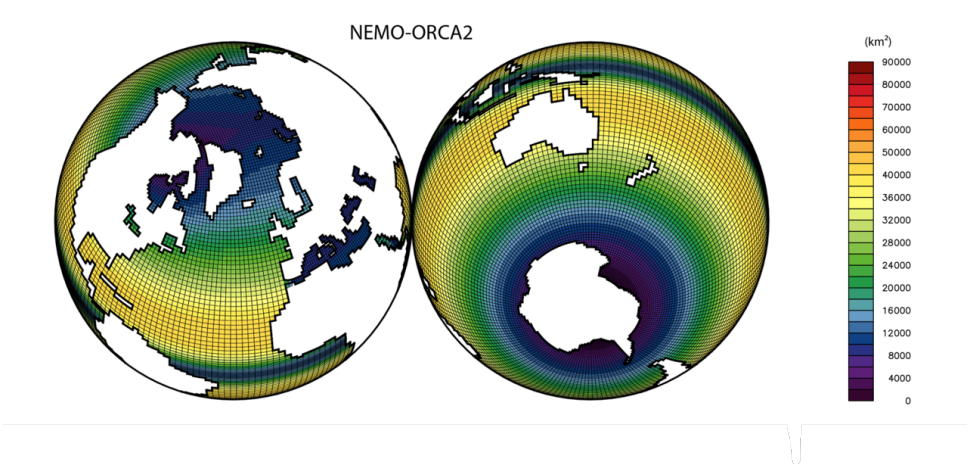

Figure 12: ORCA2 grid. Colors indicate the surface per grid cell. Figure taken from Sepulchre et al., 2020.

3.2 Model initialization

Initially, the model assumes an ocean at rest, i.e. the surface height is zero everywhere. After the first model run, the model uses the state of the ocean as the initial condition of the coming year. The model has a horizontal resolution of 2° and has z-coordinates in the vertical direction. The vertical coordinate system is the most important choice in an ocean's model (Barth, 2022; Chassignet and Malanotte-Rizzoli, 2000), since this choice is linked to the resolving of ocean processes (Griffies et al., 2000). Z-coordinates are the simplest choice for the vertical coordinate system. It divides the depth into a fixed amount of horizontal layers, where the upper ocean has typically a higher resolution than the abyssal ocean. Z-coordinates have difficulties when there is a sloping topography (see Figure 13). The model that we used had a total of 31 levels in the vertical direction. The first 15 levels increase every 10 meters, after which the resolution becomes coarser.

We did not discriminate between leap years and non-leap years. The time step for the ocean dynamics is 90 minutes, and we took 5840 steps. This results in 365 days.

In the model, we used the Equation of State of Seawater 1980 (EOS-80) (Fofonoff and Millard, 1983). This links the density to temperature, salinity and pressure and thus plays an important role in the Meridional Overturning Circulation in the Atlantic basin.

The atmospheric forcing used in the model is derived from the CORE II atmospheric forcing(Large and Yeager, 2009).

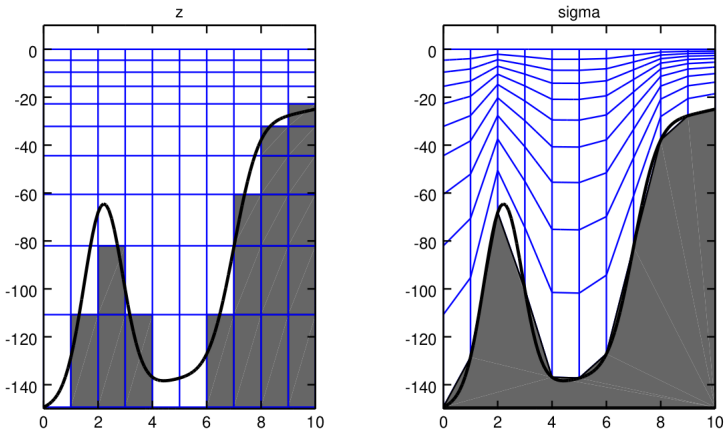

Figure 13: The left figure indicates z-coordinates. The right figure indicates sigma coordinates. Figure taken from Barth, 2022.

3.3 Mathematical formulation

3.3.1 Ocean circulation

The large-scale ocean dynamics can be modelled using the *Navier-Stokes* equations, which are partial differential equations. However, these equations are a priori not solvable and need to be simplified using additional assumptions.

The first assumption is the near incompressibility of water; this results in the Boussinesq equations. The Boussinesq equations exploit the fact that the density variations as a result of compression, thermal expansion and haline contractions, are small. The derivation (based on Vallis, 2017) goes as follows. We can write the density as the sum of a constant density (ρ_0) and a variation in density ($\delta\rho(x,y,z,t)$):

$$\rho = \rho_0 + \delta\rho(x,y,z,t).$$

Since the density variations are small, we can write:

$$|\delta\rho| << \rho_0.$$

There is a reference pressure $p_0(z)$ associated with the constant density, which is in hydrostatic balance with it. We thus have,

$$p = p_0(z) + \delta p(x,y,z,t),$$

where

$$\frac{dp_0}{dz} = -g\rho_0.$$

Since water is nearly incompressible, we can assume that density variations can be neglected, except in the gravitational term (Boussinesq equation). The equation of state is given by

$$\rho = \rho(T,S,p),$$

where T is the temperature, ρ is the density, S is the salinity and p is the pressure. The incompressibility of water leads to the simplified form of the conservation of mass:

$$\nabla \cdot U = 0, \tag{1}$$

where $\nabla\cdot$ is the divergence and U is the velocity vector. Next, we assume hydrostatic balance, i.e. the gravitational term is balanced by the pressure term. This results in the vertical momentum balance

$$\frac{\partial p}{\partial z} = -\rho g, \tag{2}$$

where p is the pressure, z is the depth, ρ is the density and g is the gravitational constant. The horizontal momentum balance is given by:

$$\frac{\partial U_h}{\partial t} = -\left[(\nabla \times U) \times U + \frac{1}{2}\nabla(U^2)\right]_h - fk \times U_h - \frac{1}{\rho_0}\nabla_h p + D^U + F^U. \tag{3}$$

We also need conservation of salt and heat, which are coupled to the velocity of the water. Conservation of heat is given by:

$$\frac{\partial T}{\partial t} = -\nabla \cdot (TU) + D^T + F^T. \tag{4}$$

and conservation of salt is given by:

$$\frac{\partial S}{\partial t} = -\nabla \cdot (SU) + D^S + F^S. \tag{5}$$

D^T, D^U and D^S is the parameterization of small-scale physics for momentum, temperature and salinity (Madec et al., 2023) and F^T, F^U and F^S are the surface forcing terms (Madec et al., 2023).

3.3.2 The meridional overturning streamfunction

The Meridional Overturning Circulation in the Atlantic basin can be calculated with the meridional overturning streamfunction (Ψ). In z-coordinates, the stream function is defined as follows:

$$\Psi(z,y) = \int_0^z \int_{x_{west}}^{x_{east}} v(x',z')dx'dz'. \tag{6}$$

This integrates the meridional velocity (v) from the bottom of the ocean to the surface and from the eastern to the western boundary. The result is transport in Sverdrup (1 Sv = 10^6 m^3/s)

3.4 Methodology

The effect of the freshwater runoff around the Antarctic continent was determined using NEMO 4.2.1, for which the source code can be found on https://forge.nemo-ocean.eu/nemo/nemo/-/releases/4.2.1. The first step consisted of the installation of NEMO, which was done via the Linux terminal. After installation, we made two configurations: one control configuration and one configuration with freshwater added. For the control configuration we used *ORCA2_ICE_PISCES*, which models the ocean circulation, sea ice and the biogeochemistry as explained in Section 3.1. *ORCA2_ICE_PISCES* needs multiple forcing and input files, such as monthly runoff, SST, bathymetry,... These files can be found on https://gws-access.jasmin.ac.uk/public/nemo/sette_inputs/. The control configuration is the standard benchmark NEMO configuration, as can be found in Madec et al., 2023.

The configuration with added freshwater was created from the control configuration. This was done by creating a new netCDF file, where we multiplied the runoff of the outer edge of the Antarctic continent by 10. This new netCDF file was used in the second configuration, which resulted in the configuration with added freshwater. The runoff around the Antarctic continent in the control configuration has values between $6.3387243 \cdot 10^{-12}$ $kgm^{-2}s^{-1}$and $2.5365644e \cdot 10^{-5}$ $kgm^{-2}s^{-1}$. Both runoff files remained the same for each month, and thus did not capture the seasonality of the runoff. Figure 15 illustrates the runoff in the control configuration and the configuration with freshwater added.

In both models, we kept the atmospheric forcing the same for each year model run. We ran each configuration for the in-simulation duration of 40 years. In total, it took us 40 days using two CPU cores to run both simulations. The simulations were done every year, where the simulation of one year had a size of approximately 5.9 gigabytes. Thus, after the first year of the simulation, we used the output of the first year as input for the ocean state in the second year. The model output were netCDF files of different temporal resolutions. The model calculated the variables such as SST, SSS, meridional velocity on a 5-day, monthly, or yearly interval. The specific model outputs that we used were sea surface salinity and temperature, surface downward heat flux and sea ice concentration.

We wanted to compute the MOC in the Atlantic basin, which we define as the Atlantic Ocean and the portion of the Southern Ocean that lies within the Atlantic sector. This could not be done directly but had to be calculated. For the calculation, we used CDFTOOLS (https://github.com/meom-group/CDFTOOLS), which is a package written in Fortran, specifically designed to analyse the output of the NEMO model. This allowed us to calculate the MOC in the Atlantic basin based on the meridional velocity component given by the model output.

The netCDF files were manipulated with the Python package *xarray*. The maps were made using the Python package *Cartopy*. To determine the impact of the added freshwater around the Antarctic continent, we always plotted the difference of the yearly or decennial average between the control configuration (C) and the configuration with added freshwater (F). In order to add some extra clarity,

$$F - C.$$

The yearly average is always based on the last year of our simulations, which is thus year 40. We did this in order to select the output which is as much in equilibrium as possible.

On these differences, we used a t-test to determine which were statistically significant. The null-hypothesis then was that two related or repeated samples had identical average (expected) values. We have a model output every 5 days, which resulted in 73 time points for an entire year. For each pixel separately, we collected the specific studied values (SST,SSS,MOC,...) , which were then stored in a vector. We thus had a vector containing all the output from the control configuration and one vector containing all the output for the freshwater one. These two vectors were then passed to the t-test, for which we stored the p-value. The p-values greater than 0.05 were discarded since they are not statistically significant. These non-statistically significant values were plotted as a mask above the original data.

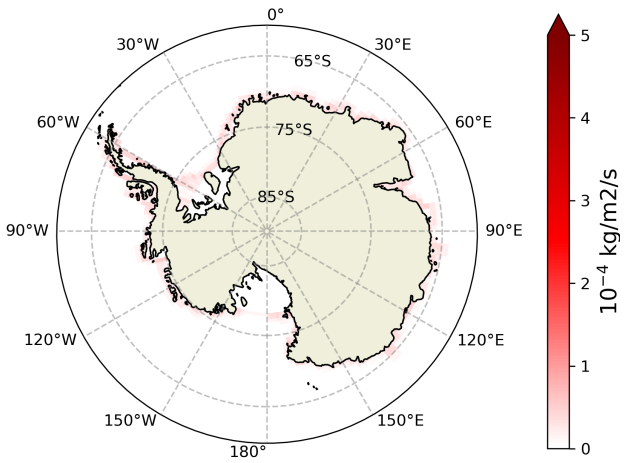

(a)

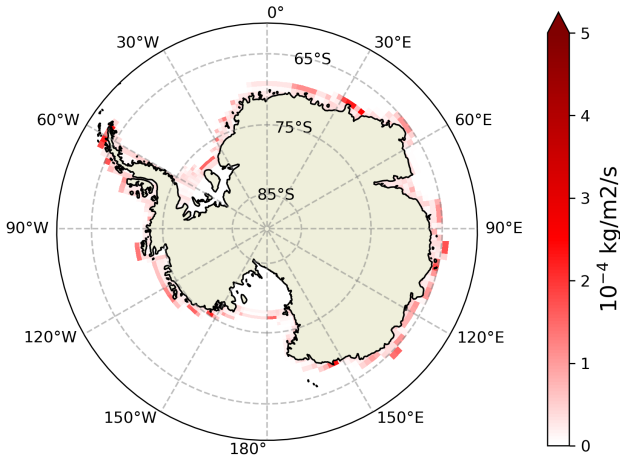

(a)

Figure 15: Figure (a) shows the control configuration. Figure (b) shows the configuration, with an increase in freshwater run-off compared to the control configuration.

4 Results

4.1 The Meridional Overturning Circulation in the Atlantic Basin

4.1.1 Yearly average transport

Figures 16 and 17 show the average Meridional Overturning Circulation in the Atlantic Basin for the last year of the simulation. Figure 18 displays the difference between the configuration with freshwater added and the control configuration. This is calculated by subtracting the output of the control configuration from the configuration with freshwater added. The gray areas indicate the statistically insignificant values ($p > 0.05$).

In Figures 16 and 17, we see the MOC in the Atlantic basin. North of 60°S, there is a clockwise circulation (in red) and an anticlockwise circulation (in blue). For the clockwise circulation, we note a volume transport of about 10 Sv (1 Sv = $10^6 m^3 s^{-1}$), while for the anticlockwise circulation, we have a volume transport of 2 Sv. South of 60°, we see an anticlockwise circulation, where the highest volume transport values are about 20 Sv.

In Figure 18, we note positive values for the approximately upper 3 km, and negative values for the approximately lower 3 km. This shows that the circulation in the upper 3 km is *stronger* in the configuration with freshwater added compared to the control configuration. This is also observed for the lower 3 km. We also notice that the most statistically insignificant values can be found around the seafloor and the highest northern latitudes.

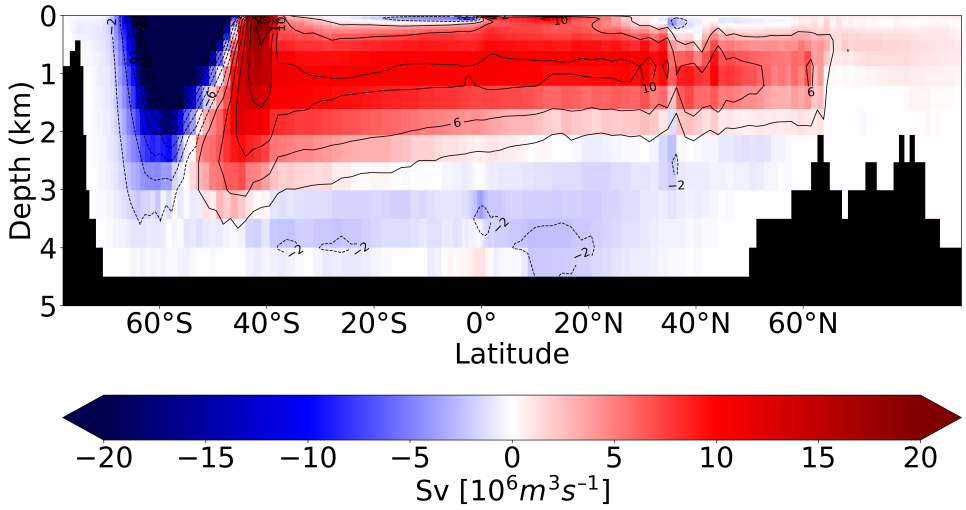

Figure 16: The yearly average Meridional Overturning Circulation in the configuration with added freshwater. The bathymetry is shown in black for all figures.

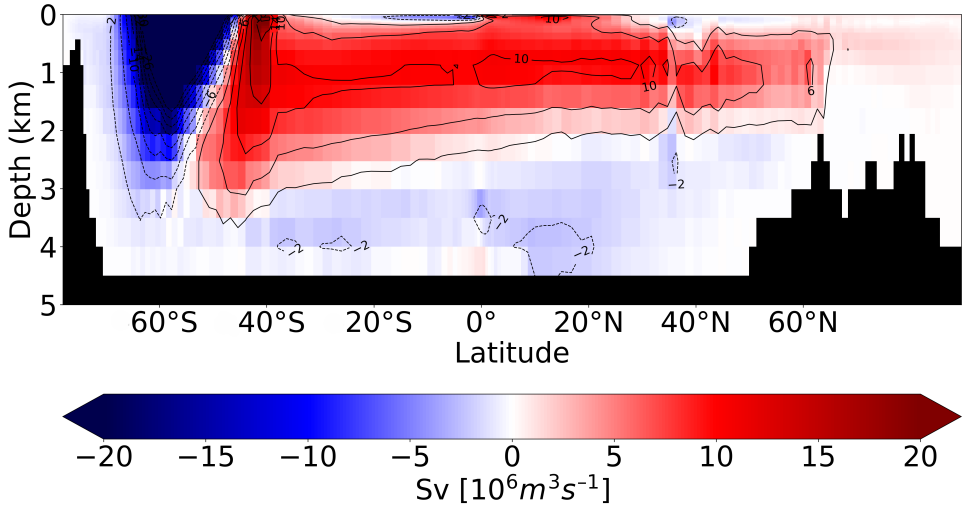

Figure 17: The yearly average Meridional Overturning Circulation in the control configuration.

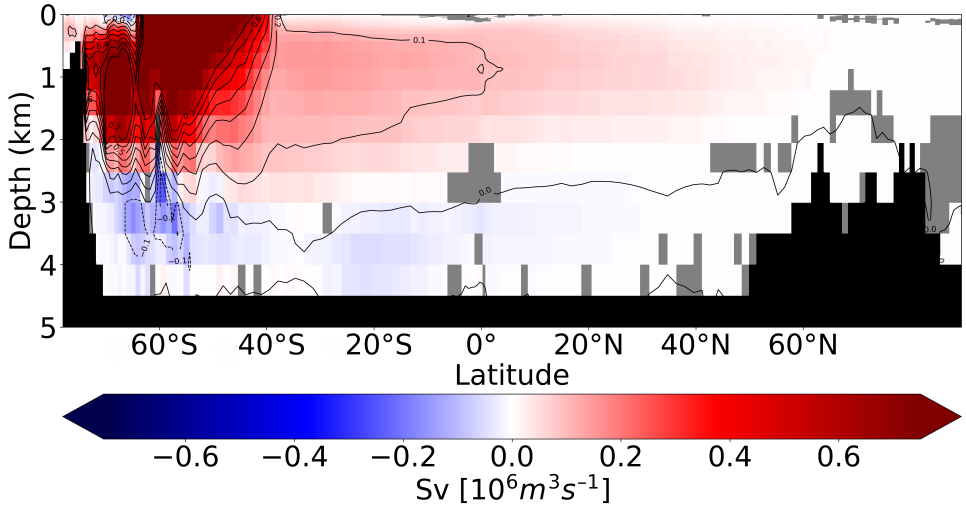

Figure 18: Difference between the yearly average of the configuration of added freshwater and the control configuration of the Meridional Overturning Circulation. The gray areas indicate the statistically insignificant values.

4.2 Time evolution of the Meridional Overturning Circulation in the Atlantic Basin

Figures 19a, 19b, and 19c show the difference for the configuration with freshwater added and the control configuration of the meridional overturning circulation in years 18, 31 and 40 respectively. The difference is calculated by subtracting the output of the control configuration from the configuration with added freshwater. We observe a contraction of the red areas from year 18 to year 31 and an expansion from year 31 to year 40. Care must be taken when interpreting this figure: depending on the region we are sometimes subtracting positive values, while in other areas we are subtracting negative values, as can be seen in Figures 16 and 17. The yearly average of the Meridional Overturning Circulation in the control configuration and the configuration with freshwater added have the same patterns as Figures 16 and 17, interannual differences cannot be observed with the naked eye.

For Figure 19a we observe a stronger circulation in the upper ocean and a weaker circulation in the lower ocean of the configuration with freshwater added compared to the control configuration. Around 60°S, we notice red and blue areas without a clear pattern.

In Figure 19b we have a contraction of the red area and an expansion of the blue area. This indicates a stronger circulation in the upper ocean of the freshwater configuration compared to the control configuration. The same trend is observed in the lower ocean. Here we additionally observe the red-blue pattern, but it becomes less pronounced than in Figure 19a.

For Figure 19c we see again an expansion of the red area, which indicates a stronger circulation in the upper part of the ocean. This is also observed for the lower part. The blue and red pattern is again becoming again pronounced.

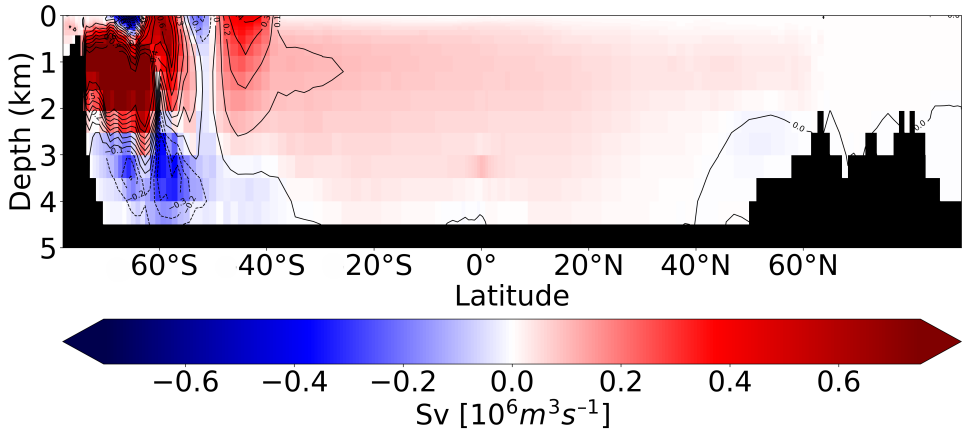

(a)

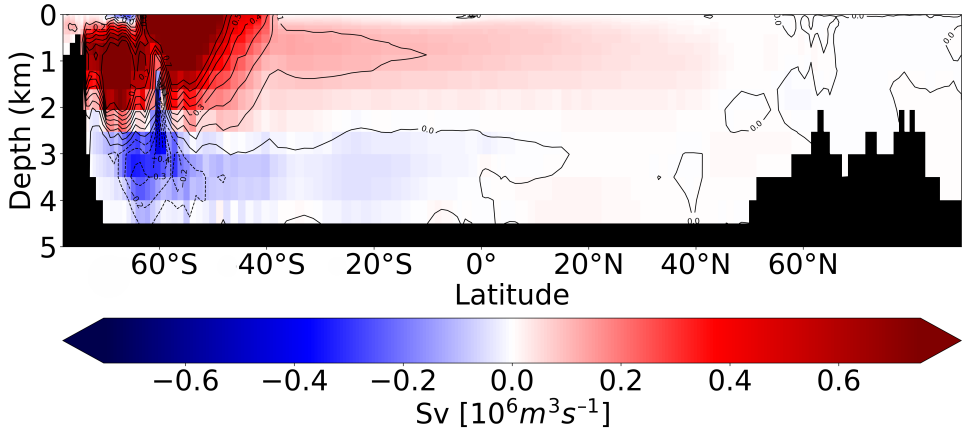

(b)

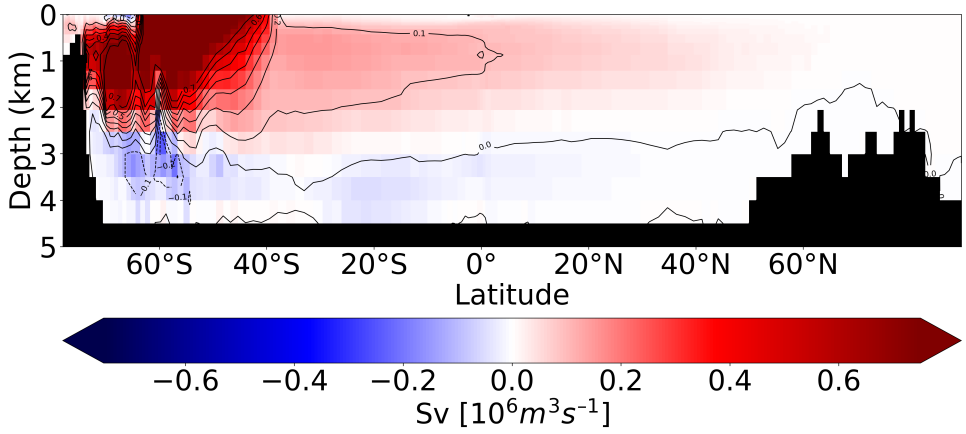

(c)

Figure 19: Time evolution of the difference in the yearly average Meridional Overturning Circulation for year 18 (a), year 31 (b) and year 40 (c). The difference is calculated by subtracting the yearly average of the control configuration from the configuration with added freshwater.

4.3 Impact on Southern Ocean

4.3.1 Yearly average of SST and SSS

Figures 20a and 20b show the differences in average sea surface temperature (SST) and sea surface salinity (SSS) between the control and freshwater-added simulations for the entire year 40, which represents the final year of the simulations. The difference is calculated by subtracting the output of the control configuration from the configuration with freshwater added. The gray areas indicate regions that are statistically insignificant, as determined by the t-test described in the methodology (see Section 3.4).

For the SST we observe negative and positive values, without a clear overall trend. The configuration with freshwater added has *lower* salinity, while the control configuration has *higher* salinity values. This results in the negative salinity values observed in Figure 20b. The highest freshening of the configuration with freshwater added occurs around the Antarctic continent and decreases outward.

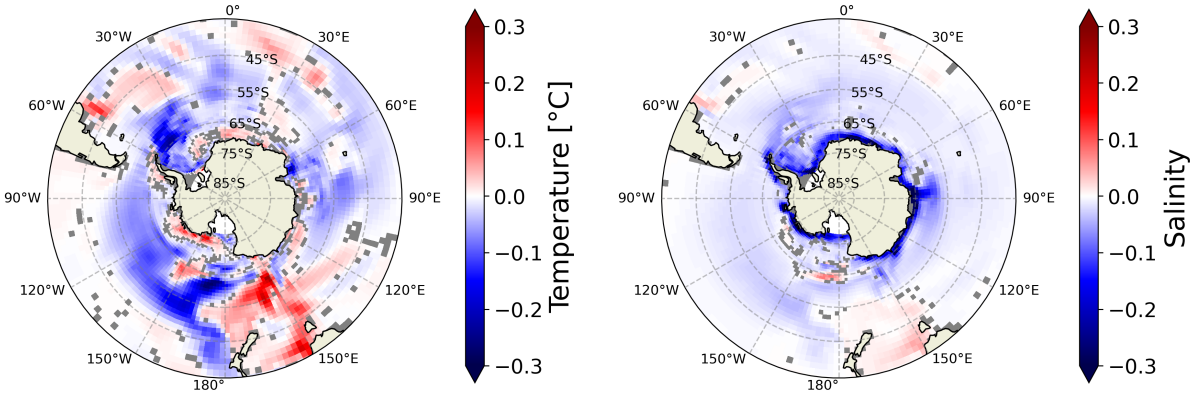

(a) (b)

Figure 20: (a) Difference in sea surface temperature (SST) between the configuration with freshwater added and the control configuration in the Southern Ocean. (b) Difference in sea surface salinity (SSS) between the configuration with freshwater added and the control configuration in the Southern Ocean. The gray areas indicate the pixels which are statistically insignificant.

4.3.2 Surface downward heat flux

Figures 21a and 21b show the average surface downward heat flux. The positive values (red) indicate the absorption of heat from the atmosphere to the ocean, the negative values (blue) indicate the release of heat from the ocean to the atmosphere. Red areas (blue areas) in Figure 21c that correspond with blue (red) areas in Figures 21a and 21b indicate that heat flux from the ocean to the atmosphere is weaker in the configuration with added freshwater compared to the control configuration. We say that there is a decrease in downward heat flux. Blue (red) areas in Figure 21c that correspond with blue (red) areas in Figures 21a and 21b indicates that heat flux from the ocean to the atmosphere is stronger in the configuration with added freshwater compared to the control configuration. We say that there is an increase in downward heat flux.

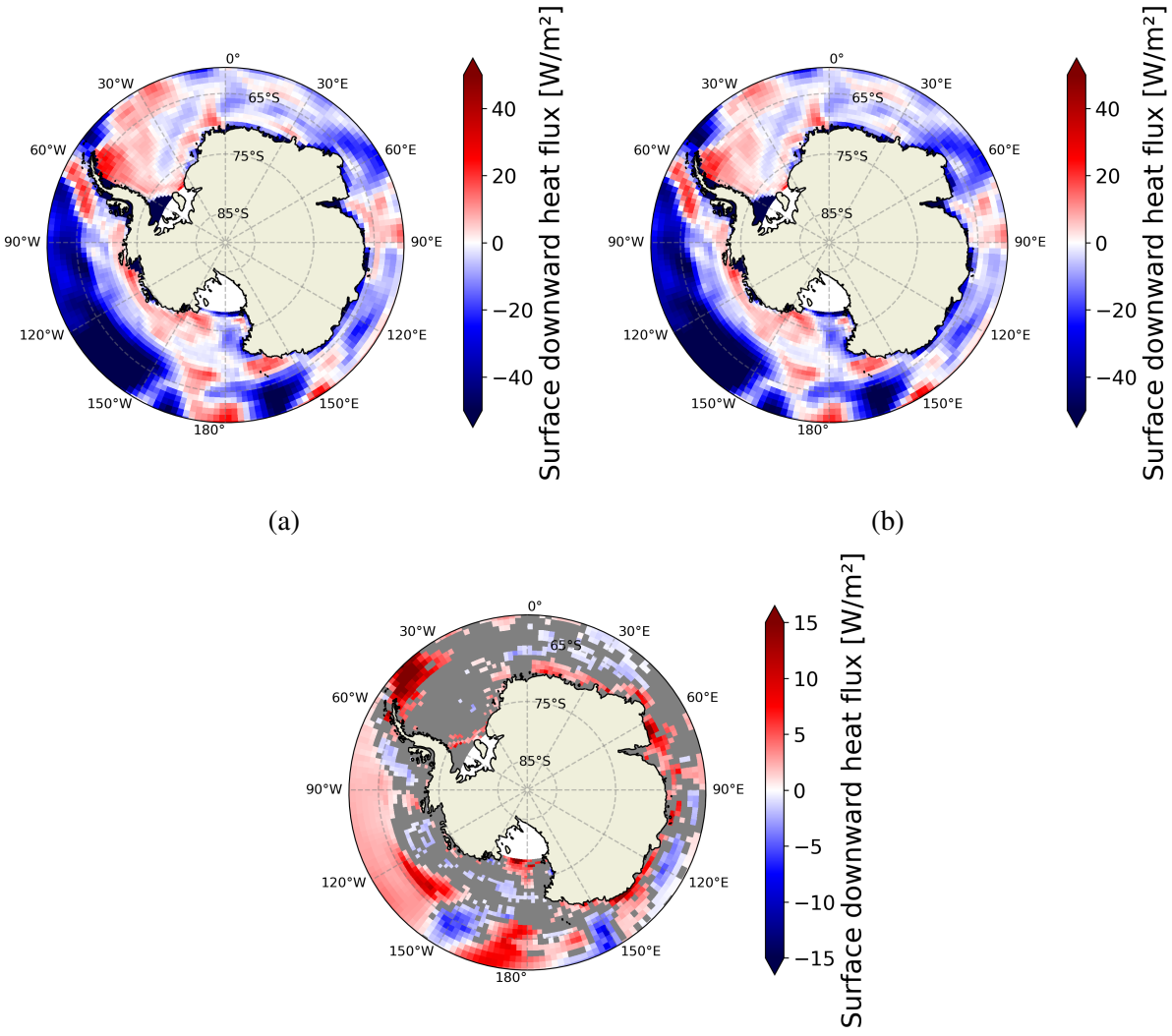

Figure 21: (a) shows the average yearly surface downward heat flux in the control configuration for year 40. (b) displays the yearly average surface downward heat flux in the configuration with added freshwater for year 40. (c) shows the difference between the average surface downward heat flux of (a) and (b). The gray areas mark the statistically insignificant zones.

4.3.3 Sea ice concentration in February and September

Figures 22 and 23 show the average sea ice concentration difference during February and September, respectively. These months are selected because February corresponds to the minimum sea ice extent, while September represents the peak sea ice coverage. The difference is calculated by subtracting the average sea ice concentration of the control configuration from the average sea ice concentration from the configuration with freshwater added.

In Figure 22a we observe an overall *increase* in sea ice concentration of the configuration with freshwater added compared to the control configuration (red areas). There is also one zone, where the sea ice concentration decreases (blue area). However, this zone is not statistically significant, as can be seen in Figure 22b.

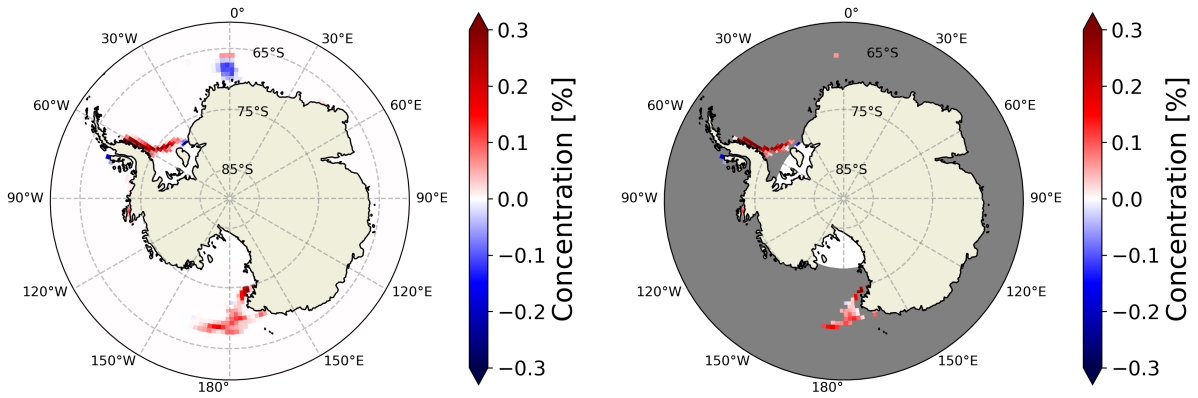

(a) (b)

Figure 22: (a) shows the difference in the average sea ice concentration in the Southern Ocean between the configuration with added freshwater and the control configuration, based on year 40. The sea ice concentration is taken from February (Austral summer), when the sea ice concentration is at a minimum. (b) adds a mask to the data given in (a) to conceal values that are not statistically significant.

In Figure 23a we also see an overall increase in average sea ice concentration of the configuration with freshwater added compared to the control configuration (red areas). There are however two blue areas, which correspond to a decrease in average sea ice concentration in the configuration with freshwater added compared to the control configuration. In this case, these areas are statistically significant, as illustrated by Fig. 23b.

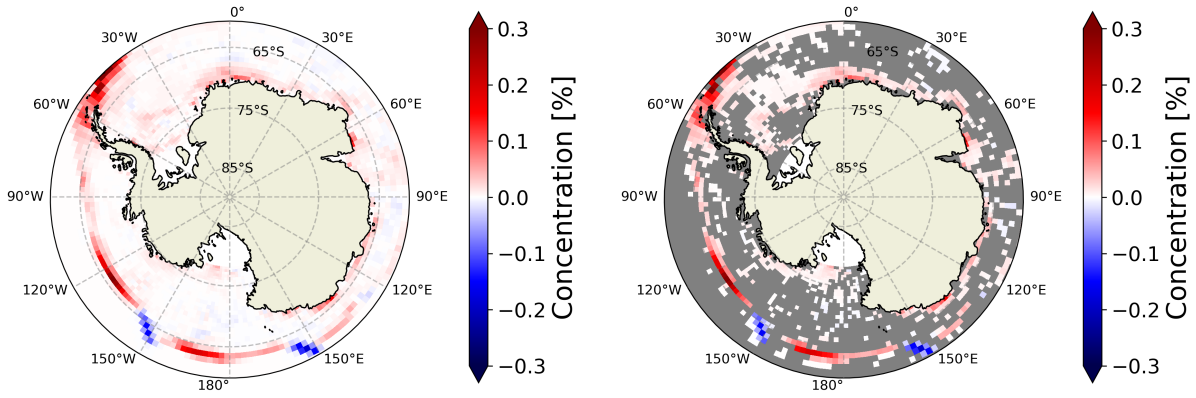

(a) (b)

Figure 23: (a) shows the difference in the average sea ice concentration in the Southern Ocean between the configuration with added freshwater and the control configuration, based on year 40. The sea ice concentration is taken from September (Austral winter) when the sea ice concentration is at a maximum. (b) adds a mask to the data given in (a) to conceal values which are not statistically significant.

4.3.4 Yearly average sea bottom temperature

Figures 24a and 24b give the average sea bottom temperature for the last year of the simulations. Figure 24c shows the difference between the averages of the sea bottom temperature, which is calculated by subtracting the output of the control configuration from the configuration with freshwater added.

In Figures 24a and 24b we observe an almost east-west distribution of sea bottom temperature; the western part shows positive temperature, while the eastern part shows negative temperature. In the Weddell Sea, Ross Sea, and around Prydz Bay, we observe the lowest sea bottom temperatures. Conversely, the highest sea bottom temperatures are found near the Antarctic continent, excluding the regions mentioned earlier. The red areas in Figure 24c indicate a warming trend in the western part of the configuration with freshwater added in comparison with the control configuration. The blue area in the Weddell Sea points to a cooling trend of the configuration with freshwater added in comparison with the control configuration.

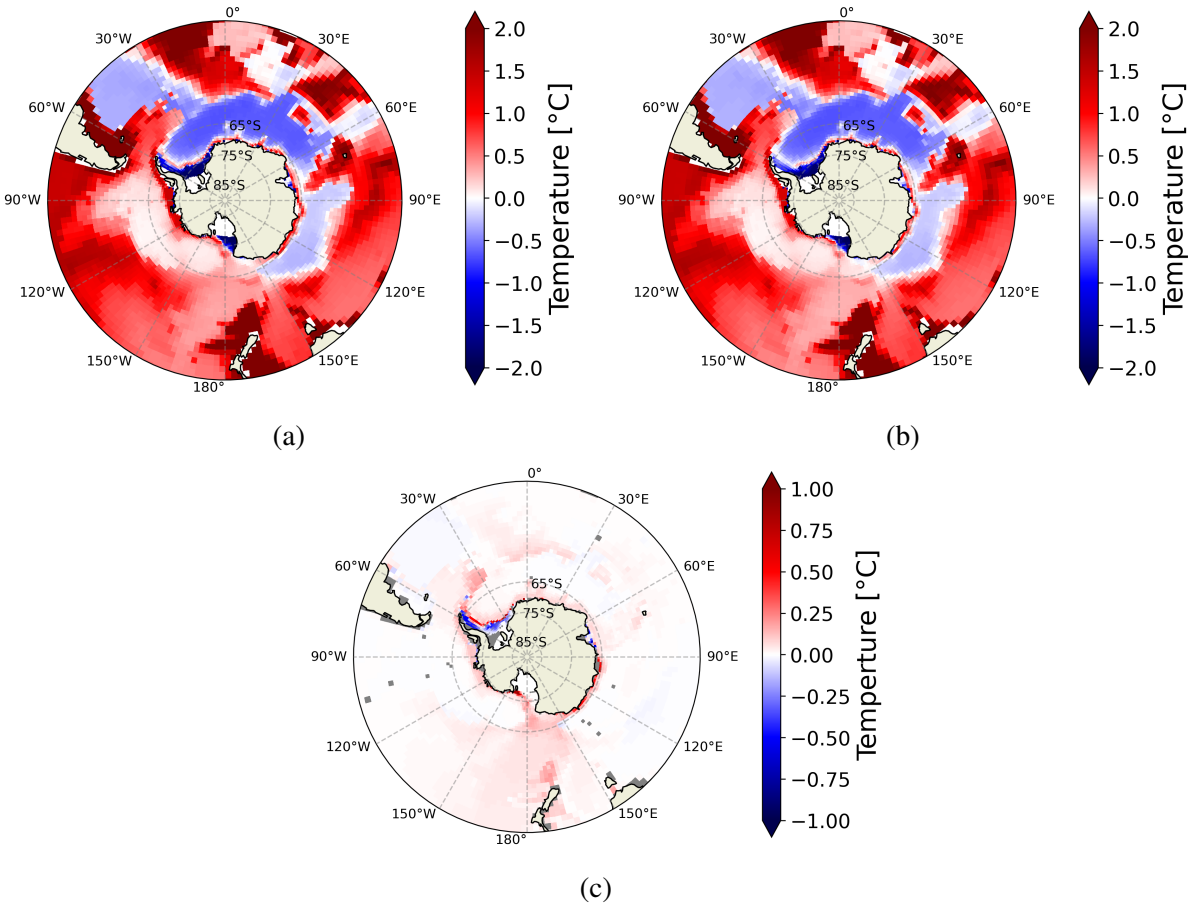

Figure 24: (a) shows the average yearly sea bottom temperature in the control configuration for year 40. (b) displays the yearly average sea bottom temperature in the configuration with added freshwater for year 40. (c) shows the difference between the average sea bottom temperature of (a) and (b). The gray areas mark the statistically insignificant zones.

4.4 Impact on global ocean

4.4.1 Yearly average of SST and SSS

Figures 25a and 25b show the difference in average yearly SST and SSS respectively. This difference is calculated by subtracting the output of the control configuration of the configuration with added freshwater. Around the Antarctic continent, we see red and blue areas *without* a clear pattern in SST and a *freshening* around the continent of the configuration with freshwater added compared to the control configuration.

In box 1, we see a blue area. This indicates that the SST in the configuration with added freshwater is *cooler* than the control configuration. Box 2 shows a *warmer* SST in the configuration with freshwater added compared to the control configuration. Around the equator in the Pacific

Ocean, in box 3, we see no clear trend in SST, although many points are statistically insignificant.

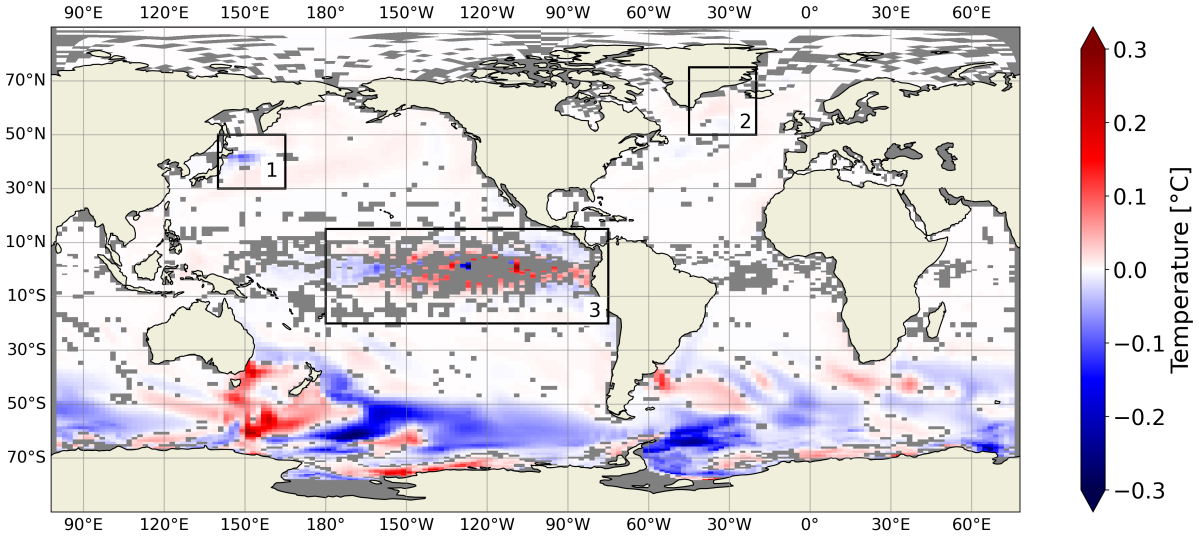

(a)

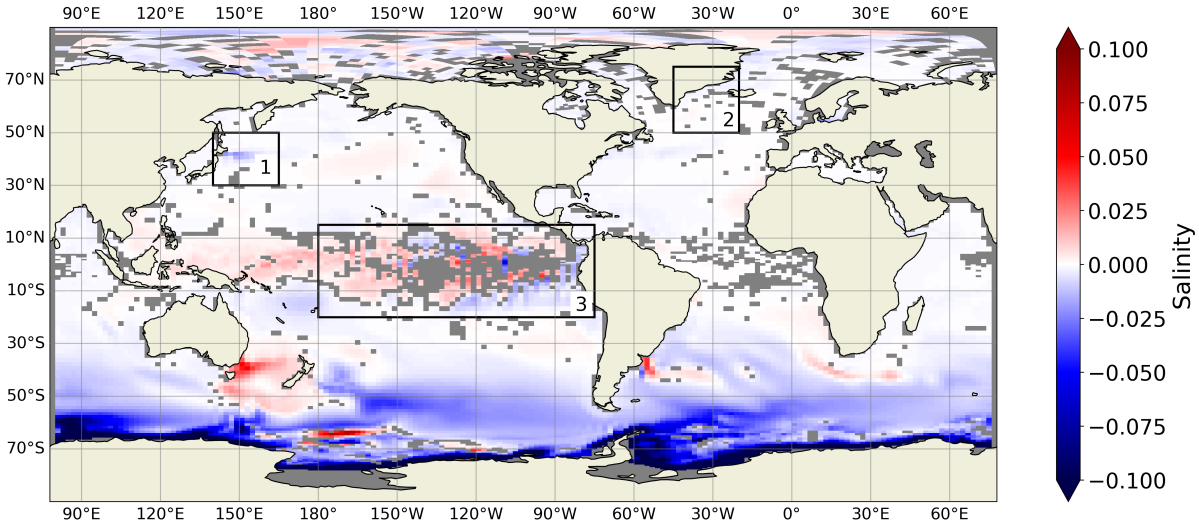

(b)

Figure 25: (a) Difference in sea surface temperature (SST) between the configuration with freshwater added and the control configuration in the global ocean. (b) Difference in sea surface salinity (SSS) between the configuration with freshwater added and the control configuration in the global ocean. Both differences are obtained from the last year of the model.

For the SSS, box 1 shows a lower SSS in the configuration with freshwater added compared to the control configuration. In Box 2 we see very faint red colours, which correspond to a higher SSS in the configuration with freshwater added compared to the control configuration. Box 3 shows again no clear trend for SSS and there are many insignificant points.

4.4.2 Yearly averaged surface downward heat flux

Figures 26a and 26b show the configuration with added freshwater and the control configuration, respectively, of the yearly averaged surface downward heat flux. Figure 26c shows the difference between the configuration with freshwater added and the control configuration, calculated by subtracting the control configuration from the freshwater one.

In box 1 on figure 26a and 26b we see that the upper part has positive values, while the lower part has negative values. Following the same reasoning as in section 4.3.2, we can that the red area corresponds to a smaller release of heat from the ocean to the atmosphere. The blue areas, in the lower part of box 1, correspond to the increase of heat from the ocean to the atmosphere.

In box 2, we find an increase in the absorption of heat compared to the control configuration. In box 3 we observe large variability in surface downward heat flux, although many values are statistically insignificant.

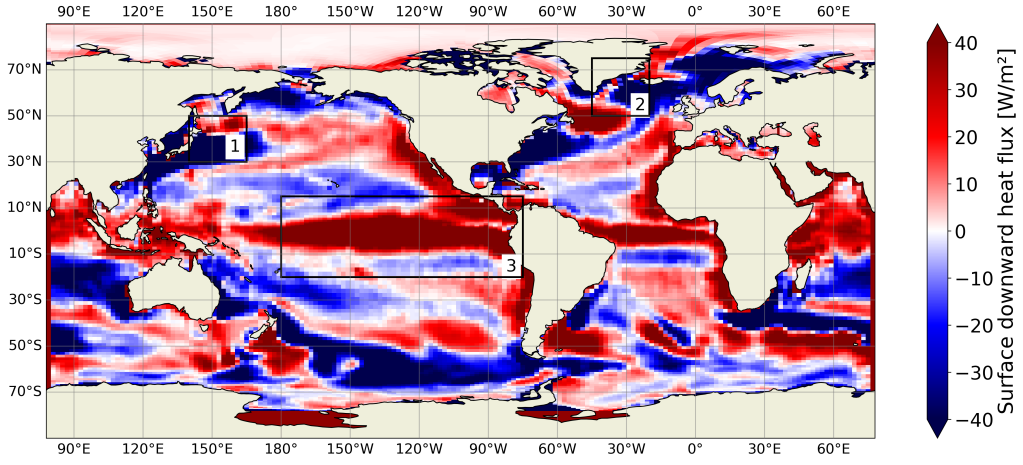

(a)

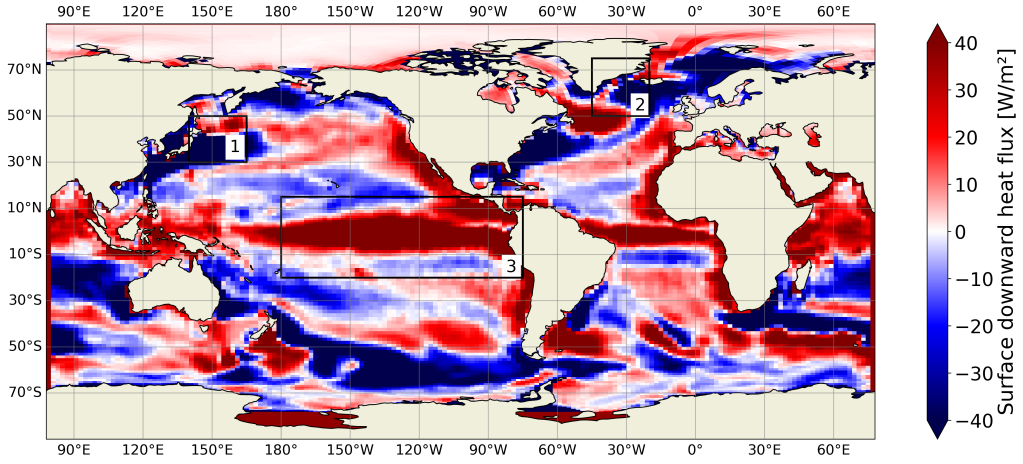

(b)

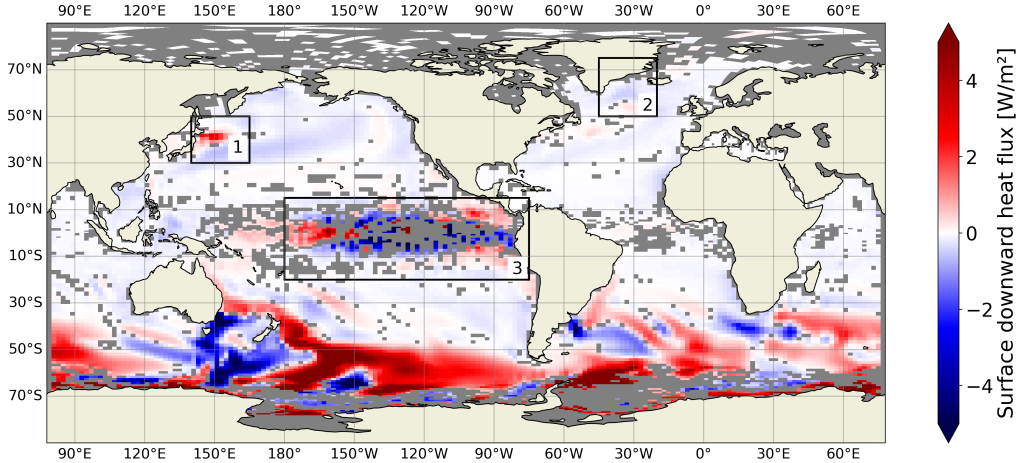

(c)

Figure 26: (a) shows the average yearly downward heat flux in the configuration with added freshwater for year 40. (b) displays the average surface downward heat flux in the control configuration for year 40. (c) shows the difference between the configuration of added freshwater (a) and the control configuration(b) of the average surface downward heat flux. The gray areas mark the statistically insignificant zones.

4.4.3 Decadal average sea surface temperature

Figures 27a and 27b give the difference SST and SSS averaged over a decade. This difference is calculated by subtracting the control configuration from the configuration with freshwater added. The gray areas indicate the p-values above 0.05.

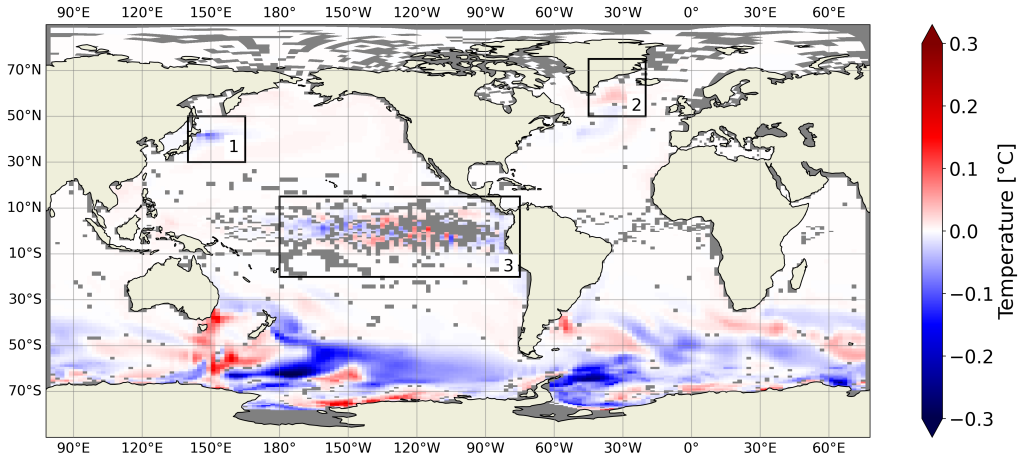

(a)

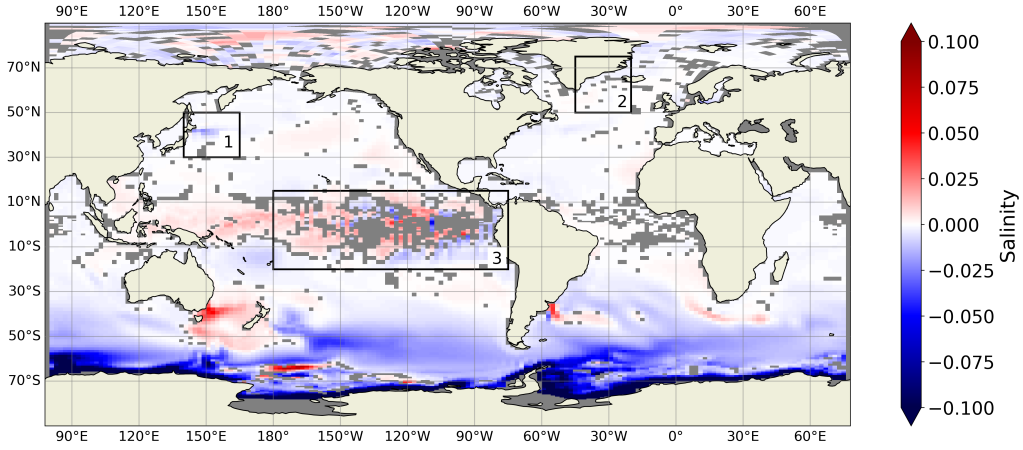

(b)

Figure 27: (a) Difference in sea surface temperature (SST) between the configuration with freshwater added and the control configuration in the global ocean for one decade. (b) Difference in sea surface salinity (SSS) between the configuration with freshwater added and the control configuration in the global ocean for one decade.

4.4.4 Yearly average sea bottom temperature

Figures 28a and 28b show the yearly average sea bottom temperature in the configuration with freshwater added and the control configuration, respectively. Figure 28c shows the difference between the configuration with freshwater added and the control configuration. We observe

an overall *increase* in sea bottom temperature of the configuration with freshwater added compared to the control configuration, except for few areas in the Southern Ocean.

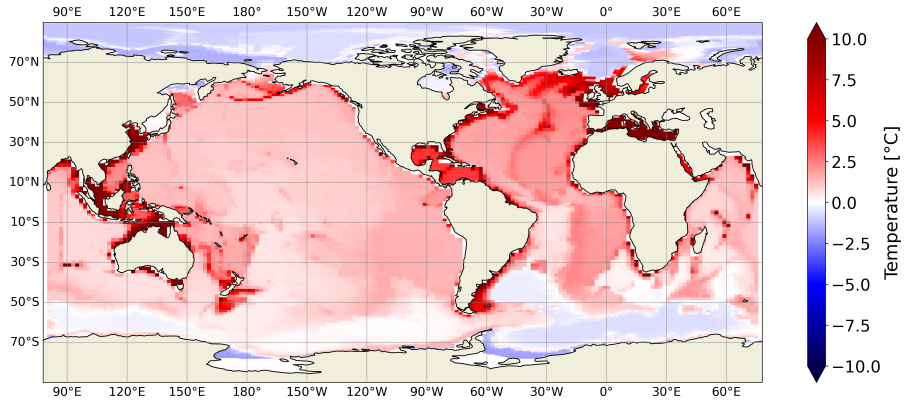

(a)

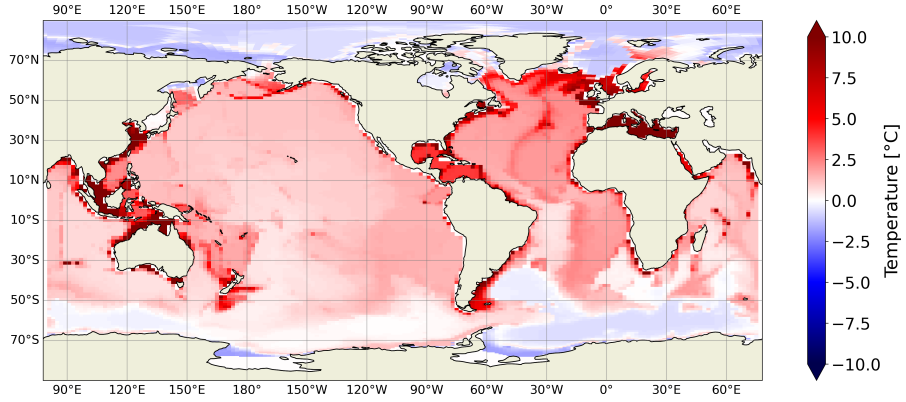

(b)

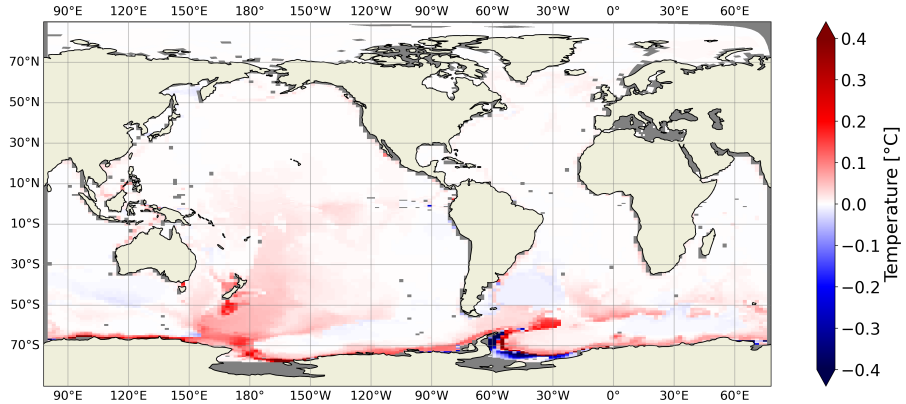

(c)

Figure 28: Figure (a) shows the average yearly sea bottom temperature in the control configuration for year 40. Figure (b) displays the yearly average sea bottom temperature in the configuration with added freshwater for year 40. Figure (c) shows the difference between the average sea bottom temperature of Figure (a) and (b). The gray areas mark the statistically insignificant zones.

5 Discussion

5.1 Comparison between the model output of the Meridional Overturning Circulation in the Atlantic Basin and observations

Figure 29 shows the observations of Meridional Overturning Circulation in the Atlantic basin. The data and the methodology are based on Lumpkin and Speer, 2007; Vallis, 2019. The figure displays a red cell, indicating a clockwise circulation primarily composed of North Atlantic Deep Water (NADW). In contrast, the blue cell indicates an anticlockwise circulation consisting of Antarctic Bottom Water (AABW). Around 40°S, a divergence caused by upwelling is observed. The contours shown on Figure 29 indicate the circulation in Sverdrup (Sv). The upper red cell has the highest values, reaching up to 16 Sv between depths of 0 and 2 km, with values decreasing outward. In contrast, the blue lower cell exhibits much smaller values, ranging between 0 and 8 Sv.

Looking at the output of the models in Figures 16 and 17, we see that the model reproduces the upper and lower cells in the Atlantic basin as seen in Figure 29. Moreover, the transports in Sverdrup have the same order as the observations: the red cell has higher values than the bottom cell. However, there are significant differences. The divergence occurs further south in the model compared to the observations, with the highest values appearing around 60°S—this is not observed in the actual data. There is also some transport in the Northern Hemisphere in the model, where the observations indicate zero transport. Furthermore, the shape of the cells differs; the red cell shrinks as it moves southward in the observations, while the opposite pattern is seen in the model output. Additionally, the deep water in the model reaches greater depths than those observed.

The discrepancy between the model and the observations can be due to various factors. Firstly, the observations show a decade average, while the model shows a one year average of observations. Secondly, the model has been running for 40 years, which can not adequately account for the deep circulation. Thirdly, due to the low-resolution of the model, the shapes of the cells are rectangular, which contributes to the more cornerlike shape.

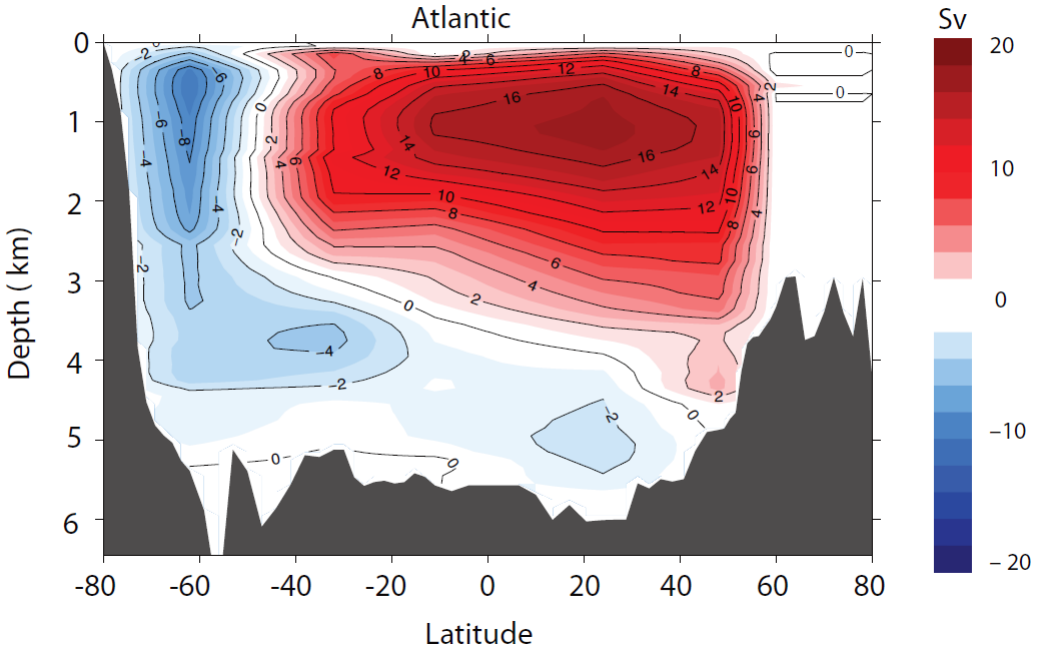

Figure 29: The Meridional Overturning Circulation in the Atlantic basin as determined by observation. The red areas indicate the clockwise circulations, while the anti-clockwise circulations are shown in blue. The upper cell, in red, corresponds mainly with North Atlantic Deep Water (NADW), while the blue cell shows Antarctic Bottom Water (AABW). Figure taken from Vallis, 2019.

5.2 Influence of freshwater on the Meridional Overturning Circulation in the Atlantic Basin

5.2.1 Time evolution

From the time evolution, as seen in figures 19a, 19b, 19c, we can make two conclusions. The first conclusion is for the upper 3 km of the ocean. We can see that the addition of freshwater makes the clockwise circulation (red values) in the upper cell stronger with time. For the lower 3 km of the ocean, we can see that the circulation in the freshwater configuration is weaker and increases with time in the lower cell. A possible explanation for this is the contraction of AABW, which lead to intrusions of the upper cell into the lower cell.

5.2.2 Comparison with literature

We find an increase in strength of the circulation in the upper cell when extra freshwater is added around the Antarctic continent. In addition, we find a decrease in AABW, which results

in a strengthening of the lower cell due to the intrusions of the upper well. This is in agreement with findings in the literature (see Lago and England, 2019; Mikolajewicz, 1998).

In the study of Mikolajewicz, 1998 the authors looked at the effect of meltwater input from the Antarctic Ice Sheet on the thermohaline circulation. This was done using a sensitivity experiment where they used an ocean general circulation model coupled to an energy-balance model of the atmosphere for 1500 years. The model had a resolution of 3.5° and 22 levels in the vertical. They found a reduction of sea surface salinity in the SO as well as deep convection which is associated with surface cooling. They also found a delayed intensification of the overturning in the Northern Hemisphere.

A more recent study by Lago and England, 2019 looked at the projected slowdown of AABW formation in response to different meltwater inputs under RCP2.6, RCP4.5, and RCP8.5. They used the Australian Community Climate and Earth System Simulator Ocean Model which had a configuration of 1° resolution in the zonal and meridional directions and 50 vertical levels (more details can be found in Lago and England, 2019). They found that the addition of freshwater leads to a slowdown in the formation rate of AABW, which reduces the ventilation of the abyssal ocean. Under RCP4.5 and RCP8.5, they concluded that there will be a near-complete shutdown of the AABW formation in 50 years. They also found that the overturning of the NADW becomes stronger, which they contribute to the SSS restoring compensation, which lead to an increase in the global SSS.

From this, we can conclude that low and high-resolution models can reproduce the effect of freshwater around the Antarctic continent. Mesoscale phenomena like eddies are less important to measure the global effect of added freshwater.

5.3 Abyssal warming

Figures 24c and 28c show an increase of average sea bottom temperature with respect to the control configuration. From this, we deduce a warming of the sea bottom water when there is an increase in freshwater around the Antarctic continent, consistent with observations of

warming of the abyssal ocean (Purkey and Johnson, 2010). This is also consistent with abyssal warming, as has also been found in the results of the model by Li et al., 2023. Here they used a high horizontal resolution of 0.1°. In this study, they found that under increasing meltwater forcing, the abyssal ocean warms. This is a result of the contraction of the AABW, which enables warmer CDW to reach into the abyssal ocean (Li et al., 2023).

5.4 Yearly vs decadal SST and SSS

If we compare Figures 25a and 27a, we see that the overall SST (SSS) is similar for the yearly and decadal SST (SSS). We notice that the statistically insignificant area decreases in the decadal average; this is a result of the nature of any statistical hypothesis test that exactly compares means, such as the t-test. If we have a larger period, the test statistic and p-value will be lower.

The biggest difference in SST and SSS can be found in box 2 (North Atlantic) on 25a and 27a. We find a stronger SST and SSS signal in the decadal average, while we do not notice significant change in SST and SSS in box 1 (North Pacific) and box 3 (Equatorial Pacific). This means that the signal in the SST and SSS in the region of box 1 is stronger per decade than per year.

5.5 Sea ice concentration and ecosystems

As a result of increasing freshwater, we observe an increase in sea ice concentration. This is in agreement with observations (Comiso and Nishio, 2008) and can be explained due to the fact that more freshwater on the surface, freezes more easily and thus leads to more sea ice.

An increase in sea ice concentration can have a profound impact on marine ecosystems, since sea ice plays an important role as a habitat for organisms and provides nutrients and shelter for the organisms living in sea ice (Arrigo and Thomas, 2004). For example, it could affect the Adélie Penguin (*Pygoscelis adeliae*), one of the most abundant predators in Antarctica (Maccapan et al., 2023). This penguin depends on prey which live in the sea ice (Maccapan et al., 2023), so a change in sea ice could influence their diet. Another example can be found in sea-

ice algae. When the ice melts, these algae are released from the sea ice, after which they sink (Selz et al., 2018), affecting the biological pump. We can thus conclude that sea ice variability has an important effect on ecosystems in the Southern Ocean and also on the export of carbon.

5.6 Anomalies in the equatorial Pacific and the north Pacific

For the global SST (Figure 20a) and SSS (Figure 20b), the influence of the added freshwater remains largely contained around the SO, however there are three places (box 1, box 2 and box 3) that have an important effect.

5.6.1 Warm Blob?

A possible sign of a *slowing* down of the Atlantic Meridional Overturning circulation is a cold blob in the subpolar North Atlantic, as can be seen in Figure 30. This warming hole (Drijfhout et al., 2012) is an observed feature in today's SST, while the SST of the global ocean is rising. This area corresponds to deep water formation in the Irminger Sea. This anomaly is also observed in the net heat loss, as shown on the left of Figure 30.

In our results (see box 2, Figure 25a) we observe the opposite: An increase in SST in the freshwater configuration compared to the control configuration and a decrease of the surface downward heat flux. This could be a sign of the reversed effect: due to an enhancement of the Atlantic Meridional Overturning we could have an increase in warmer, saltier water which arrives in the Irminger Sea and leads to an increase in the AMOC.

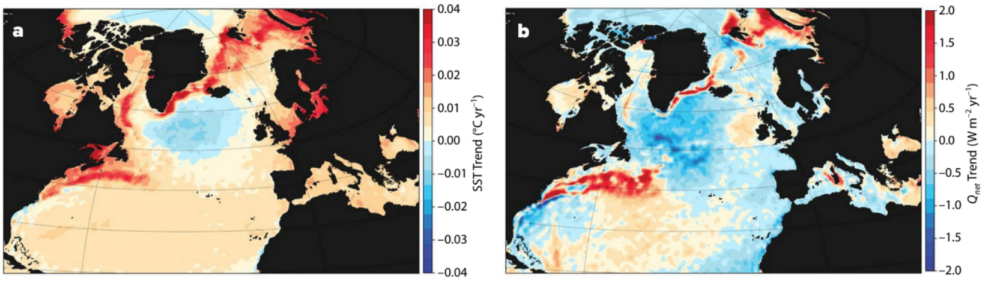

Figure 30: The left figure show the SST trend. Figure taken from Rahmstorf, 2023.

5.6.2 The equatorial Pacific

Box 3 in Figures 25a, 25b, 27a, and 27b shows the equatorial Pacific. This region corresponds with the Niño region as can be seen on Figure 31. El Niño Southern Oscillation (ENSO) is a climate phenomenon which has three states: El Niño, La Niña and a neutral state. It affects weather globally, leading to unusual dry and warm conditions in South East Asia, Southern Africa and Australia and increased rainfall in the southern United States and the Horn of Africa. It also affects global economic growth (Callahan and Mankin, 2023) and has major implications for human health. Similarly, El Niño is linked to cholera risk in Bangladesh and malaria epidemics in parts of South Asia and America (Kovats et al., 2003).

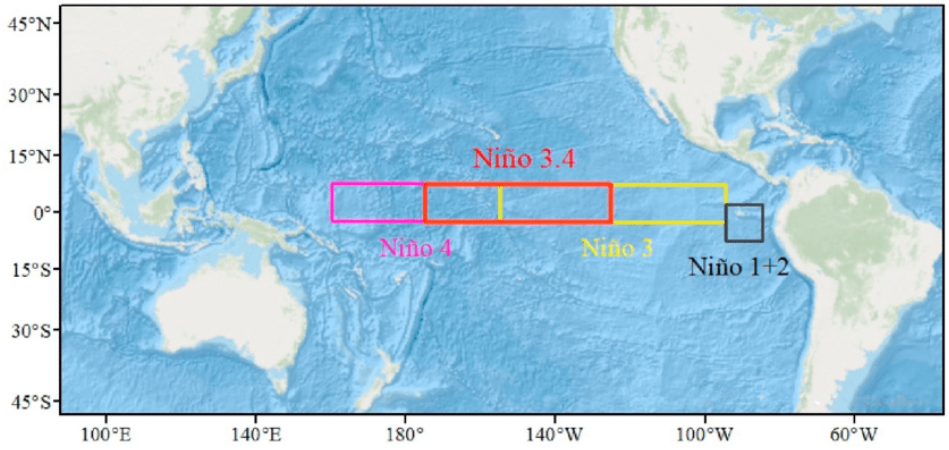

Figure 31: Outline of Niño regions. Figure taken from (Wang et al., 2021)

Once there are five consecutive 3-month running mean of SST anomalies in the Ninõ 3.4 (see Figure 31) region above/below the threshold of +0.5°C (-0.5°C) in the equatorial Pacific, there is an El Niño/La Niña (National Centers for Environmental Information (NCEI), 2024).

Statistically, there is a weak signal in box 3 (Equatorial Pacific), as indicated by the prevalence of gray pixels. However, this does not imply that there is no underlying physical process. In Orihuela-Pinto et al., 2022 they studied the ENSO variability under a collapsed AMOC, which they explain as a result of the air-sea coupling. However, since the atmospheric forcing is the same in both simulations, we need to look for an explanation elsewhere, which is solely due to the ocean currents.

A potential explanation to explain this anomaly is the Humboldt current, which is mainly wind-driven. Our hypothesis is that the addition of freshwater in the SO is advected by wind-driven gyres to the equatorial Pacific (see Figure 32). As can be viewed in Figure 32, we see that the freshwater signal could be advected under the influence of the ACC, which then ends up in the Humboldt current. The scattered pattern (red and blue) can then be explained as a result of the yearly average, since the meltwater pulses vary from year to year. Looking at the SSS anomaly (25b) and comparing this with Figure 32, we see that our advection by wind-driven gyres could be plausible, since there are blue colors at the lower part of box 3, which indicate lower SSS and thus more freshwater.

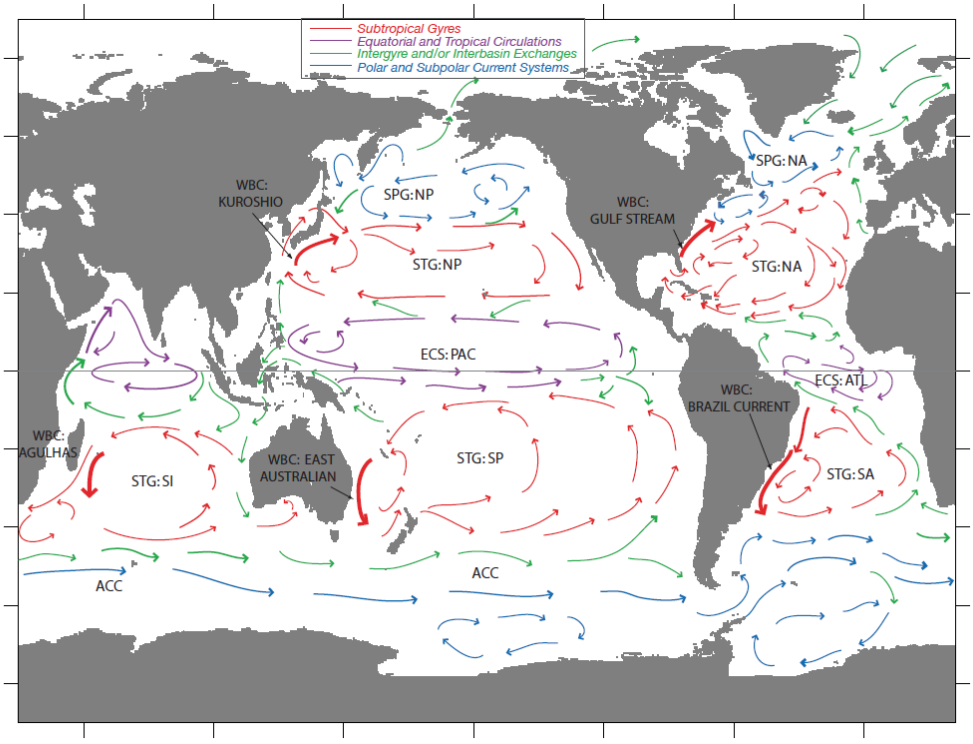

Figure 32: Idealisation of the Wind-driven currents. STG – Subtropical Gyre; SPG – Subpolar Gyre; WBC – Western Boundary Current; ECS – Equatorial Current System; NA – North Atlantic; SA – South Atlantic; NP – North Pacific; SP – South Pacific; SI – South Indian; ACC – Antarctic Circumpolar Current; ATL – Atlantic; PAC – Pacific. Figure taken from Vallis, 2017.

5.6.3 North Pacific

In box 1 (North Pacific) on Figures 25a and 25b, we see that the freshwater configuration has cooler and fresher water in the region of the Kuroshio current. This is a statistically significant signal. We have the following hypothesis for explaining this signal: around the equator, we have observed a strong signal in anomalous SST and SSS. This signal is then transported via the equatorial Current System (purple arrow, in equatorial Pacific) towards the north, as can be seen on Figure 32. Via interbasin exchanges (green arrows) this signal is then advected towards the Kuroshio current, which lead to the observed signal in SST and SSS.

6 Conclusion and future work

Although we used a low-resolution model over a relatively short time, we were able to replicate the same qualitative results as in higher resolution models. We found that an increase in freshwater around the Antarctic continent indeed affects the Meridional Overturning Circulation in the Atlantic basis. More specifically, for the upper part, it leads to an enhancement of the upper meridional overturning circulation. For the lower part, it results in a reduction of AABW. This could have important implications for marine ecosystems and biogeochemical cycling around the globe.

We also found that the sea surface temperature, sea surface salinity, sea bottom temperature and surface downward heat flux are altered by increased meltwater in the Southern Ocean. It has a warming effect for the abyssal ocean. For the surface ocean, we identified three regions with anomalous behavior. The warming blob in the North Atlantic indicates the enhancement of the upper circulation. Besides this, the anomalous behavior in the North Pacific and the Equatorial Pacific can be explained by wind-driven gyres. The signal in the Equatorial Pacific could have an important effect on ENSO. This indicates the importance of the Southern Ocean on global scales. Moreover, we found an increase in sea ice concentration, which has important effects on sea ice biology.

Although our work highlights the importance of meltwater around Antarctica for global ocean circulation, climate and ecosystems, it has important shortcomings. Firstly, we ran the model only for 40 years, which is a short timescale to capture the behavior of the AABW. Running the model for longer would make it possible to draw more realistic conclusions about AABW formation. Secondly, we used EOS-80 as the Equation of State of Seawater, which is replaced by TEOS-10. This could affect density variations and thus impact our results. Thirdly, we did not account for seasonality in runoff. This assumption is not realistic, since the runoff is highly variable interseasonally and interannually (Tuckett et al., 2021). Lastly, we did not make use of in-situ data in order to validate our model.

Due to the length constraints, we were not able to analyze the biogeochemical output of the model, which could be done in future work. As mentioned, this work did not use realistic values of runoff, however it highlights the importance thereof. Since meltwater in the Southern Ocean not only has a regional effect, but is globally felt. Therefore, it is crucial to represent the Antarctic meltwater realistically in coupled climate models, to understand the role it plays on global ocean circulation and climate (Purich and England, 2023), which could be done in future work.

We could also repeat this methodology for realistic runoff under different Shared Socio-economic Pathways (SSP) (Intergovernmental Panel on Climate Change (IPCC), 2022). This would enable us to see how the meridional overturning circulation in the Atlantic Basin would change under the influence of realistic freshwater runoff, under different scenarios, which corresponds to different increases in global temperature. In addition, we could also run models at high-resolution to investigate in detail what happens in the North Atlantic, North Pacific and Equatorial Pacific. Moreover, we could use recent satellite and in-situ observations to compare the newest observations with model output.

References

Arrigo, R., Kevin, & Thomas, D. N. (2004). Large scale importance of sea ice biology in the Southern Ocean. *Antarctic Science*, *16*(4), 471–486. https://doi.org/10.1017/S0954102004002263

Atamanchu, D. (2021). Linking Oxygen and Carbon Uptake with the Meridional Overturning Circulation Using a Transport Mooring Array. *Oceanography*. https://doi.org/10.5670/oceanog.2021.supplement.02-03

Barth, A. (2022, September). Structure and application of numerical ocean models. https://github.com/gher-uliege/OCEA0036

Bintanja, R., van Oldenborgh, G. J., Drijfhout, S., Wouters, B., & Katsman, C. (2013). Important role for ocean warming and increased ice-shelf melt in Antarctic sea-ice expansion. *Nature Geoscience*, *6*(5), 376–379. https://doi.org/10.1038/ngeo1767

Bronselaer, B., Winton, M., Griffies, S. M., Hurlin, W. J., Rodgers, K. B., Sergienko, O. V., Stouffer, R. J., & Russell, J. L. (2018). Change in future climate due to Antarctic meltwater. *Nature*, *564*(7734), 53–58. https://doi.org/10.1038/s41586-018-0712-z

Callahan, C. W., & Mankin, J. S. (2023). Persistent effect of El Niño on global economic growth. *Science*, *380*(6649), 1064–1069. https://doi.org/10.1126/science.adf2983

Chapman, C. C., Lea, M.-A., Meyer, A., Sallée, J.-B., & Hindell, M. (2020). Defining Southern Ocean fronts and their influence on biological and physical processes in a changing climate. *Nature Climate Change*, *10*(3), 209–219. https://doi.org/10.1038/s41558-020-0705-4

Charrassin, J.-B., Hindell, M., Rintoul, S. R., Roquet, F., Sokolov, S., Biuw, M., Costa, D., Boehme, L., Lovell, P., Coleman, R., Timmermann, R., Meijers, A., Meredith, M., Park, Y.-H., Bailleul, F., Goebel, M., Tremblay, Y., Bost, C.-A., McMahon, C. R., … Guinet, C. (2008). Southern Ocean frontal structure and sea-ice formation rates revealed by elephant seals. *Proceedings of the National Academy of Sciences*, *105*(33), 11634–11639. https://doi.org/10.1073/pnas.0800790105

Chassignet, E. P., & Malanotte-Rizzoli, P. (Eds.). (2000). *Dynamics of Atmospheres and Oceans (special issue)* (Vol. 32). Elsevier Science.

Cheng, W., Chiang, J. C. H., & Zhang, D. (2013). Atlantic Meridional Overturning Circulation (AMOC) in CMIP5 Models: RCP and Historical Simulations. *Journal of Climate*, *26*(18), 7187–7197. https://doi.org/10.1175/JCLI-D-12-00496.1

Comiso, J. C., & Nishio, F. (2008). Trends in the sea ice cover using enhanced and compatible AMSR-E, SSM/I, and SMMR data. *Journal of Geophysical Research: Oceans*, *113*(C2). https://doi.org/10.1029/2007JC004257

de Lavergne, C., Palter, J. B., Galbraith, E. D., Bernardello, R., & Marinov, I. (2014). Cessation of deep convection in the open Southern Ocean under anthropogenic climate change. *Nat. Climate Change*, *4*, 278–282. https://doi.org/10.1038/nclimate2132

de Lavergne, C., Madec, G., Roquet, F., Holmes, R., & Mcdougall, T. J. (2017). Abyssal ocean overturning shaped by seafloor distribution. *Nature*, *551*(7679), 181–186. https://doi.org/10.1038/nature24472

Ditlevsen, P., & Ditlevsen, S. (2023). Warning of a forthcoming collapse of the Atlantic meridional overturning circulation. *Nature Communications*, *14*(1), 1–12. https://doi.org/10.1038/s41467-023-39810-w

Dong, S., Sprintall, J., Gille, S. T., & Talley, L. (2008). Southern Ocean mixed-layer depth from Argo float profiles. *Journal of Geophysical Research: Oceans*, *113*(C6). https://doi.org/10.1029/2006JC004051

Dorschel, B., Hehemann, L., Viquerat, S., Warnke, F., Dreutter, S., Tenberge, Y. S., Accettella, D., An, L., Barrios, F., Bazhenova, E., et al. (2022). The international bathymetric chart of the Southern Ocean version 2. *Scientific Data*, *9*(1), 275. https://doi.org/10.1038/s41597-022-01366-7

Drijfhout, S., Van Oldenborgh, G. J., & Cimatoribus, A. (2012). Is a decline of AMOC causing the warming hole above the North Atlantic in observed and modeled warming patterns? *Journal of Climate*, *25*(24), 8373–8379. https://doi.org/10.1175/JCLI-D-12-00490.1

Durack, P. J., & Wijffels, S. E. (2010). Fifty-year trends in global ocean salinities and their relationship to broad-scale warming. *J. Climate*, *23*, 4342–4362. https://doi.org/10.1175/2010JCLI3377.1

Durack, P. J., Wijffels, S. E., & Matear, R. J. (2012). Ocean salinities reveal strong global water cycle intensification during 1950 to 2000. *Science*, *336*, 455–458. https://doi.org/10.1126/science.1212222

Fofonoff, N. P., & Millard, R. C. (1983). Algorithms for computation of fundamental properties of seawater. *UNESCO Technical Papers in Marine Science. Documents techniques de l'Unesco sur les sciences de la mer*. https://doi.org/10.25607/OBP-1450

Foster, T. D., & Carmack, E. C. (1976). Frontal zone mixing and Antarctic Bottom Water formation in the southern Weddell Sea. *Deep Sea Research and Oceanographic Abstracts*, *23*(4), 301–317.

Frölicher, T. L., Sarmiento, J. L., Paynter, D. J., Dunne, J. P., Krasting, J. P., & Winton, M. (2015). Dominance of the Southern Ocean in anthropogenic carbon and heat uptake in CMIP5 models. *Journal of Climate*, *28*(2), 862–886. https://doi.org/10.1175/JCLI-D-14-00117.1

Garabato, A. C. N., Polzin, K. L., Ferrari, R., Zika, J. D., & Forryan, A. (2016). A microscale view of mixing and overturning across the Antarctic Circumpolar Current. *Journal of Physical Oceanography*, *46*(1), 233–254. https://doi.org/10.1175/JPO-D-15-0025.1

Gill, A., Green, J., & Simmons, A. (1974). Energy partition in the large-scale ocean circulation and the production of mid-ocean eddies. *Deep sea research and oceanographic abstracts*, *21*(7), 499–528. https://doi.org/10.1016/0011-7471(74)90010-2

Gordon, A. L. (1982). Weddell Deep Water variability. *Journal of Marine Research*, *40*.

Gordon, A. L. (1986). Interocean exchange of thermocline water. *Journal of Geophysical Research: Oceans*, *91*(C4), 5037–5046. https://doi.org/10.1029/JC091iC04p05037

Gordon, A. L. (2009). Bottom water formation. *Ocean currents*, *263*, 269. https://doi.org/10.1016/B978-012374473-9.00006-0

Griffies, S. M., Böning, C., Bryan, F. O., Chassignet, E. P., Gerdes, R., Hasumi, H., Hirst, A., Treguier, A.-M., & Webb, D. (2000). Developments in ocean climate modelling. *Ocean Modelling*, *2*, 123–192. https://doi.org/10.1016/S1463-5003(00)00014-7

Group, N. T. W. (2018). TOP – Tracers in Ocean Paradigm – The NEMO Tracers engine. https://doi.org/10.5281/ZENODO.1471700

Intergovernmental Panel on Climate Change (IPCC). (2022). *Climate Change 2022: Impacts, Adaptation, and Vulnerability* (H.-O. Pörtner, D. Roberts, M. Tignor, E. Poloczanska, K. Mintenbeck, A. Alegría, M. Craig, S. Langsdorf, S. Löschke, V. Möller, A. Okem, & B. Rama, Eds.). Cambridge University Press. https://doi.org/10.1017/9781009325844

Jacobs, S. S., Amos, A. F., & Bruchhausen, P. M. (1970). Ross Sea oceanography and Antarctic bottom water formation. *Deep Sea Research and Oceanographic Abstracts*, *17*(6), 935–962. https://doi.org/10.1016/0011-7471(70)90046-X

Johnson, G. C. (2008). Quantifying Antarctic bottom water and North Atlantic deep water volumes. *Journal of Geophysical Research: Oceans*, *113*(C5). https://doi.org/10.1029/2007JC004477

Khatiwala, S., Primeau, F., & Hall, T. (2009). Reconstruction of the history of anthropogenic CO2 concentrations in the ocean. *Nature*, *462*(7271), 346–349. https://doi.org/10.1038/nature08526

Killworth, P. D. (1979). On "chimney" formations in the ocean. *Journal of Physical Oceanography*, *9*(3), 531–554. https://doi.org/10.1175/1520-0485(1979)009⟨0531:OFITO⟩2.0.CO;2

Killworth, P. D. (1983). Deep convection in the World Ocean. *Reviews of Geophysics*, *21*(1), 1–26. https://doi.org/10.1029/RG021i001p00001

Kim, S.-K., Kim, H.-J., Dijkstra, H. A., & An, S.-I. (2022). Slow and soft passage through tipping point of the Atlantic Meridional Overturning Circulation in a changing climate. *npj Climate and Atmospheric Science*, *5*(1), 13. https://doi.org/10.1038/s41612-022-00236-8

Konrad, H., Shepherd, A., Gilbert, L., Hogg, A. E., McMillan, M., Muir, A., & Slater, T. (2018). Net retreat of Antarctic glacier grounding lines. *Nature Geoscience*, *11*(4), 258–262. https://doi.org/10.1038/s41561-018-0082-z

Kovats, R. S., Bouma, M. J., Hajat, S., Worrall, E., & Haines, A. (2003). El Niño and health. *The Lancet*, *362*(9394), 1481–1489. https://doi.org/10.1016/s0140-6736(03)14695-8

Lago, V., & England, M. H. (2019). Projected slowdown of Antarctic bottom water formation in response to amplified meltwater contributions. *Journal of Climate*, *32*(19), 6319–6335. https://doi.org/10.1175/JCLI-D-18-0622.1

Large, W., & Yeager, S. (2009). The global climatology of an interannually varying air–sea flux data set. *Climate dynamics*, *33*, 341–364. https://doi.org/10.1007/s00382-008-0441-3

Lenton, T. M., Held, H., Kriegler, E., Hall, J. W., Lucht, W., Rahmstorf, S., & Schellnhuber, H. J. (2008). Tipping elements in the Earth's climate system. *Proceedings of the*

national Academy of Sciences, *105*(6), 1786–1793. https://doi.org/10.1073/pnas.070541410

Li, Q., England, M. H., Hogg, A. M., Rintoul, S. R., & Morrison, A. K. (2023). Abyssal ocean overturning slowdown and warming driven by Antarctic meltwater. *Nature*, *615*(7954), 841–847. https://doi.org/10.1038/s41586-023-05762-w

Lumpkin, R., & Speer, K. (2007). Global ocean meridional overturning. *Journal of Physical Oceanography*, *37*(10), 2550–2562. https://doi.org/10.1175/JPO3130.1

Lynch-Stieglitz, J. (2017). The Atlantic meridional overturning circulation and abrupt climate change. *Annual review of marine science*, *9*, 83–104. https://doi.org/10.1146/annurev-marine-010816-060415

Maccapan, D., Careddu, G., Calizza, E., Sporta Caputi, S., Rossi, L., & Costantini, M. L. (2023). Effects of Sea-Ice Persistence on the Diet of Adélie Penguin (Pygoscelis adeliae) Chicks and the Trophic Differences between Chicks and Adults in the Ross Sea, Antarctica. *Biology*, *12*(5). https://doi.org/10.3390/biology12050708

Madec, G., Bell, M., Blaker, A., Bricaud, C., Bruciaferri, D., Castrillo, M., Calvert, D., Jérômeme Chanut, Clementi, E., Coward, A., Epicoco, I., Éthé, C., Ganderton, J., Harle, J., Hutchinson, K., Iovino, D., Lea, D., Lovato, T., Martin, M., … Wilson, C. (2023). NEMO Ocean Engine Reference Manual. https://doi.org/10.5281/ZENODO.8167700

Manabe, S., Stouffer, R. J., Spelman, M. J., & Bryan, K. (1991). Transient responses of a coupled ocean–atmosphere model to gradual changes of atmospheric CO2. Part I. Annual mean response. *Journal of Climate*, *4*(8), 785–818. https://doi.org/10.1175/1520-0442(1991)004⟨0785:TROACO⟩2.0.CO;2

Marinov, I., Gnanadesikan, A., Toggweiler, J., & Sarmiento, J. L. (2006). The southern ocean biogeochemical divide. *Nature*, *441*(7096), 964–967. https://doi.org/10.1038/nature04883

Marshall, J., Donohoe, A., Ferreira, D., & McGee, D. (2014). The ocean's role in setting the mean position of the Inter-Tropical Convergence Zone. *Climate Dynamics*, *42*, 1967–1979. https://doi.org/10.1007/s00382-013-1767-z

Marshall, J., & Speer, K. (2012). Closure of the meridional overturning circulation through Southern Ocean upwelling. *Nature geoscience*, *5*(3), 171–180. https://doi.org/10.1038/ngeo1391

Martin, E. R., Thorncroft, C., & Booth, B. B. (2014). The multidecadal Atlantic SST—Sahel rainfall teleconnection in CMIP5 simulations. *Journal of Climate*, *27*(2), 784–806. https://doi.org/10.1175/JCLI-D-13-00242.1

Marzocchi, A., & Jansen, M. F. (2019). Global cooling linked to increased glacial carbon storage via changes in Antarctic sea ice. *Nature geoscience*, *12*(12), 1001–1005. https://doi.org/10.1038/s41561-019-0466-8

Meredith, M. P., Schofield, O., Newman, L., Urban, E., & Sparrow, M. (2013). The vision for a Southern Ocean observing system. *Current Opinion in Environmental Sustainability*, *5*(3-4), 306–313. https://doi.org/10.1016/j.cosust.2013.03.002

Mikaloff-Fletcher, S. E., Gruber, N., Jacobson, A. R., Doney, S. C., Dutkiewicz, S., Gerber, M., Follows, M., Joos, F., Lindsay, K., Menemenlis, D., et al. (2006). Inverse estimates of anthropogenic CO2 uptake, transport, and storage by the ocean. *Global Biogeochemical Cycles*, *20*(2). https://doi.org/10.1029/2005GB002530

Mikolajewicz, U. (1998). Effect of meltwater input from the Antarctic ice sheet on the thermohaline circulation. *Annals of Glaciology*, *27*, 311–315. https://doi.org/10.3189/1998AoG27-1-311-315

Munk, W. H. (1966). Abyssal recipes. *Deep Sea Research and Oceanographic Abstracts*, *13*(4), 707–730. https://doi.org/10.1016/0011-7471(66)90602-4

National Centers for Environmental Information (NCEI). (2024). Equatorial Pacific Sea Surface Temperatures (SST) [Accessed: August 21, 2024]. https://www.ncei.noaa.gov/access/monitoring/enso/sst

Ohshima, K. I., Fukamachi, Y., Williams, G. D., Nihashi, S., Roquet, F., Kitade, Y., Tamura, T., Hirano, D., Herraiz-Borreguero, L., Field, I., et al. (2013). Antarctic Bottom Water production by intense sea-ice formation in the Cape Darnley polynya. *Nature Geoscience*, *6*(3), 235–240. https://doi.org/doi.org/10.1038/ngeo1738

Orihuela-Pinto, B., Santoso, A., England, M. H., & Taschetto, A. S. (2022). Reduced ENSO variability due to a collapsed Atlantic Meridional Overturning Circulation. *Journal of Climate*, *35*(16), 5307–5320. https://doi.org/10.1175/JCLI-D-21-0293.1

Paolo, F. S., Fricker, H. A., & Padman, L. (2015). Volume loss from Antarctic ice shelves is accelerating. *Science*, *348*(6232), 327–331. https://doi.org/10.1126/science.aaa0940

Parish, T. R., & Bromwich, D. H. (1997). On the forcing of seasonal changes in surface pressure over Antarctica. *Journal of Geophysical Research: Atmospheres*, *102*(D12), 13785–13792. https://doi.org/10.1029/96JD02959

Petit, T., Lozier, M. S., Josey, S. A., & Cunningham, S. A. (2020). Atlantic deep water formation occurs primarily in the Iceland Basin and Irminger Sea by local buoyancy forcing. *Geophysical Research Letters*, *47*(22), e2020GL091028. https://doi.org/10.1029/2020GL091028

Pritchard, H., Ligtenberg, S. R., Fricker, H. A., Vaughan, D. G., van den Broeke, M. R., & Padman, L. (2012). Antarctic ice-sheet loss driven by basal melting of ice shelves. *Nature*, *484*(7395), 502–505. https://doi.org/10.1038/nature10968

Purich, A., & England, M. H. (2023). Projected Impacts of Antarctic Meltwater Anomalies over the Twenty-First Century. *Journal of Climate*, *36*(8), 2703–2719. https://doi.org/10.1175/JCLI-D-22-0457.1

Purkey, S. G., & Johnson, G. C. (2010). Warming of global abyssal and deep Southern Ocean waters between the 1990s and 2000s: Contributions to global heat and sea level rise budgets. *Journal of Climate*, *23*(23), 6336–6351. https://doi.org/10.1175/2010JCLI3682.1

Rahmstorf, S. (2002). Ocean circulation and climate during the past 120,000 years. *Nature*, *419*(6903), 207–214. https://doi.org/10.1038/nature01090

Rahmstorf, S. (2023). Is the Atlantic Overturning Circulation approaching a tipping point? *XXVIII General Assembly of the International Union of Geodesy and Geophysics (IUGG)*. https://doi.org/10.5670/oceanog.2024.501

Reid, J. L. (1994). On the total geostrophic circulation of the North Atlantic Ocean: Flow patterns, tracers, and transports. *Progress in Oceanography*, *33*(1), 1–92. https://doi.org/10.1016/0079-6611(94)90014-0

Robinson, A., & Stommel. (1959). The Oceanic Thermocline and the Associated Thermohaline Circulation. *Tellus*, *11*(3), 295–308. https://doi.org/10.1111/j.2153-3490.1959.tb00035.x

Rudels, B., & Quadfasel, D. (1991). Convection and deep water formation in the Arctic Ocean-Greenland Sea system. *Journal of Marine Systems*, *2*(3-4), 435–450. https://doi.org/10.1016/0924-7963(91)90045-V

Sarmiento, J. L., Gruber, N., Brzezinski, M., & Dunne, J. (2004). High-latitude controls of thermocline nutrients and low latitude biological productivity. *Nature*, *427*(6969), 56–60. https://doi.org/10.1038/nature02127

Selz, V., Lowry, K. E., Lewis, K. M., Joy-Warren, H. L., van de Poll, W., Nirmel, S., Tong, A., & Arrigo, K. R. (2018). Distribution of Phaeocystis antarctica-dominated sea ice algal communities and their potential to seed phytoplankton across the western Antarctic Peninsula in spring. *Marine Ecology Progress Series*, *586*, 91–112. https://doi.org/10.3354/meps12367

Sepulchre, P., Caubel, A., Ladant, J.-B., Bopp, L., Boucher, O., Braconnot, P., Brockmann, P., Cozic, A., Donnadieu, Y., Dufresne, J.-L., Estella-Perez, V., Ethé, C., Fluteau, F., Foujols, M.-A., Gastineau, G., Ghattas, J., Hauglustaine, D., Hourdin, F., Kageyama, M., & Tardif, D. (2020). IPSL-CM5A2 - An Earth system model designed for multi-millennial climate simulations. *Geoscientific Model Development*, *13*, 3011–3053. https://doi.org/10.5194/gmd-13-3011-2020

Sigman, D. M., & Boyle, E. A. (2000). Glacial/interglacial variations in atmospheric carbon dioxide. *Nature*, *407*(6806), 859–869. https://doi.org/10.1038/35038000

Silvano, A., Purkey, S., Gordon, A. L., Castagno, P., Stewart, A. L., Rintoul, S. R., Foppert, A., Gunn, K. L., Herraiz-Borreguero, L., Aoki, S., et al. (2023). Observing Antarctic bottom water in the Southern Ocean. *Frontiers in Marine Science*, *10*, 1221701. https://doi.org/10.3389/fmars.2023.1221701

Sinet, S., von der Heydt, A. S., & Dijkstra, H. A. (2023). AMOC Stabilization Under the Interaction With Tipping Polar Ice Sheets [e2022GL100305 2022GL100305]. *Geophysical Research Letters*, *50*(2), e2022GL100305. https://doi.org/10.1029/2022GL100305

Skliris, N., Marsh, R., Josey, S. A., Good, S. A., Liu, C., & Allan, R. P. (2014). Salinity changes in the World Ocean since 1950 in relation to changing surface freshwater fluxes. *Climate dynamics*, *43*, 709–736. https://doi.org/10.1007/s00382-014-2131-7

Speer, K., Rintoul, S. R., & Sloyan, B. (2000). The diabatic Deacon cell. *Journal of Physical Oceanography*, *30*(12), 3212–3222. https://doi.org/10.1175/1520-0485(2000)030⟨3212:TDDC⟩2.0.CO;2

Stommel, H. (1958). The abyssal circulation. *Deep Sea Research*, *5*(1), 80–82. https://doi.org/10.1016/S0146-6291(58)80014-4

Sutton, R. T., & Hodson, D. L. (2005). Atlantic Ocean forcing of North American and European summer climate. *Science*, *309*(5731), 115–118. https://doi.org/10.1126/science.1109496

Svendsen, L., Kvamstø, N. G., & Keenlyside, N. (2014). Weakening AMOC connects equatorial Atlantic and Pacific interannual variability. *Climate dynamics*, *43*, 2931–2941. https://doi.org/0.1007/s00382-013-1904-8

Swart, N. C., Gille, S. T., Fyfe, J. C., & Gillett, N. P. (2018). Recent Southern Ocean warming and freshening driven by greenhouse gas emissions and ozone depletion. *Nature Geoscience*, *11*(11), 836–841. https://doi.org/10.1038/s41561-018-0226-1

Talley, L. D. (2011). *Descriptive physical oceanography: An introduction*. Academic press.

Talley, L. D. (2013). Closure of the global overturning circulation through the Indian, Pacific, and Southern Oceans: Schematics and transports. *Oceanography*, *26*(1), 80–97. https://doi.org/10.5670/oceanog.2013.07

The IMBIE team. (2018). Mass balance of the Antarctic Ice Sheet from 1992 to 2017. *Nature*, *558*(7709), 219–222. https://doi.org/10.1038/s41586-018-0179-y

Thompson, A. F., Stewart, A. L., Spence, P., & Heywood, K. J. (2018). The Antarctic Slope Current in a changing climate. *Reviews of Geophysics*, *56*(4), 741–770. https://doi.org/10.1029/2018RG000624

Trenberth, K. E., Zhang, Y., Fasullo, J. T., & Cheng, L. (2019). Observation-based estimates of global and basin ocean meridional heat transport time series. *Journal of Climate*, *32*(14), 4567–4583. https://doi.org/10.1002/rog.20022

Tuckett, P. A., Ely, J. C., Sole, A. J., Lea, J. M., Livingstone, S. J., Jones, J. M., & van Wessem, J. M. (2021). Automated mapping of the seasonal evolution of surface meltwater and its links to climate on the Amery Ice Shelf, Antarctica. *The Cryosphere*, *15*(12), 5785–5804. https://doi.org/10.5194/tc-15-5785-2021

Vallis, G. K. (2017). *Atmospheric and Oceanic Fluid Dynamics: Fundamentals and Large-Scale Circulation* (2nd ed.). Cambridge University Press. https://doi.org/10.1017/9781107588417

Vallis, G. K. (2019). *Essentials of Atmospheric and Oceanic Dynamics*. Cambridge University Press. https://doi.org/10.1017/9781107588431

Vancoppenolle, M., Rousset, C., Blockley, E., Aksenov, Y., Feltham, D., Fichefet, T., Garric, G., Guémas, V., Iovino, D., Keeley, S., Madec, G., Massonnet, F., Ridley, J., Schroeder, D., & Tietsche, S. (2023). SI3, the NEMO Sea Ice Engine. https://doi.org/10.5281/ZENODO.7534900

van Westen, R. M., Kliphuis, M., & Dijkstra, H. A. (2024). Physics-based early warning signal shows that AMOC is on tipping course. *Science advances*, *10*(6), eadk1189. https://doi.org/10.1126/sciadv.adk118

Wadhams, P., Holfort, J., Hansen, E., & Wilkinson, J. (2002). A deep convective chimney in the winter Greenland Sea. *Geophysical Research Letters*, *29*(10), 76–1. https://doi.org/10.1029/2001GL014306

Wang, S., Mu, L., & Liu, D. (2021). A hybrid approach for El Niño prediction based on Empirical Mode Decomposition and convolutional LSTM Encoder-Decoder. *Computers Geosciences*, *149*, 104695. https://doi.org/10.1016/j.cageo.2021.104695

Warren, B. A. (1983). Why is no deep water formed in the North Pacific? *Journal of Marine Research*, *41*(2), 327–347. https://doi.org/10.1016/0198-0254(83)96395-1

Weaver, A. J., Sedláček, J., Eby, M., Alexander, K., Crespin, E., Fichefet, T., Philippon-Berthier, G., Joos, F., Kawamiya, M., Matsumoto, K., Steinacher, M., Tachiiri, K., Tokos, K., Yoshimori, M., & Zickfeld, K. (2012). Stability of the Atlantic meridional overturning circulation: A model intercomparison. *Geophysical Research Letters*, *39*(20). https://doi.org/10.1029/2012GL053763

Weijer, W., Cheng, W., Garuba, O. A., Hu, A., & Nadiga, B. T. (2020). CMIP6 Models Predict Significant 21st Century Decline of the Atlantic Meridional Overturning Circulation. *Geophysical Research Letters*, *47*(12), e2019GL086075. https://doi.org/10.1029/2019GL086075

Williams, G., Bindoff, N., Marsland, S., & Rintoul, S. (2008). Formation and export of dense shelf water from the Adélie Depression, East Antarctica. *Journal of Geophysical Research: Oceans*, *113*(C4). https://doi.org/10.1029/2007JC004346

Worby, A. P., Geiger, C. A., Paget, M. J., Van Woert, M. L., Ackley, S. F., & DeLiberty, T. L. (2008). Thickness distribution of Antarctic sea ice. *Journal of Geophysical Research: Oceans*, *113*(C5). https://doi.org/10.1029/2007JC004254

Wouters, B., Martin-Español, A., Helm, V., Flament, T., van Wessem, J. M., Ligtenberg, S. R., Van den Broeke, M. R., & Bamber, J. L. (2015). Dynamic thinning of glaciers on the Southern Antarctic Peninsula. *Science*, *348*(6237), 899–903. https://doi.org/10.1126/science.aaa5727